Arctic Alaska barrier Islands: improving the fidelity of morphological impact predictions

Phase 1

Ahmed Elghandour
Dano Roelvink

IHE Delft

August 2020

Table of Contents

List of Figures

List of Tables

Abstract

In light of the concerns due to climate change and sea-level rise, there is a need to predict future stability and evolution of barrier islands in Arctic Alaska. For such dynamic areas, in terms of the computational cost, reduced complexity models are preferred to carry out long term simulations. The new free-form coastline model ShorelineS that is capable to describe large coastal transformations (Roelvink et al., 2020), was selected to simulate the changes in the barrier islands. It was hypothesized that the main drivers to the changes are alongshore transport gradient, overwash and wave refraction. Such processes are schematized in the model.

Four barrier islands were chosen to replicate their geomorphic behavior. These are: Reindeer, Cross, Narwhal, and Stockton islands. The simulations were performed using the historical shorelines, hindcast waves and bathymetry. Also, a routine was added into the model to update the bathymetry when needed, a scale factor was introduced to control the barrier overwash process, and a 2D wave solver was used to transmit and refract the waves. In order to calibrate the model and determine the influential parameters, based on the available data and the user experience, a range of values of the model parameters were defined. First, the values were tested with the four barriers in the period from the 2000s to 2010s. Then additional tests were performed for Cross island in the period from 2006 to 2009 to evaluate the sensitivity of the model parameters.

The modelled and the observed shorelines were compared. Modelling results show that the 2D wave solver, overwash and bathymetry updates routines leads to more realistic results. The most influential parameters are closure depth, spit width, and surf width (where the model obtains the wave conditions for the longshore transport formula). The model was capable to capture the barrier rollover and spit growing processes. However, further work is necessary to the following. First, to test additional modifications that might improve the resultse such as different alongshore transport formula, and reduced grid size for the bathymetry. Second, including the ice impact which was neglected in this study. Third, further analysis of available data to quantify the main processes controlling the coastal changes. Finally, using the data assimilation technique to auto-calibrate the model and improve the result.

1 Introduction

1.1 Objective

This report is a part of task 4.5.3 (Barrier Island Morphology and Recovery) of the USGS-Deltares cooperative research project (11204520). The project by USGS that aims to project future stability and evolution of barrier islands along the Alaska Arctic coast (from Norton Sound to the Canadian border).

This study was requested to extend USGS research on Alaskan barrier islands through a numerical study of five barrier islands within Stefansson Sound and Foggy Island Bay, located in the western Beaufort Sea along the northern Alaskan coast (Figure 1).

The study aims to develop and calibrate the ShorelineS model to simulate the behavior of a series of barrier islands in Arctic Alaska.

1.2 Outline of the report

This report first describes the data used in this study (Chapter 2). Then the model is described including the main processes, the model setup including the essential parameters, and the model performance evaluation (Chapter 3). In Chapter 4 the simulations for the four barrier islands and the additional sensitivity tests are presented and discussed. The preliminary conclusions and recommendations for further research are presented in Chapter 5.

2 Arctic Alaska Barrier Islands

2.1 Study area

Barrier islands along the Alaskan Arctic coast accommodate a high percentage of the open-ocean exposed coast. Therefore, they protect the mainland from open ocean waves approaching the coast, and they provide sheltering habitats for species such as shorebirds. The types of barrier islands along this coast can be grouped into remnant barrier islands, typically with a tundra core and recently formed barrier islands and spits commonly attached to the remnant barriers (Gibbs et al., 2018). The migration rates of the barrier islands have changed along the coast over the past 60 years, ranging from 50 m to 1 km. Four barrier islands were selected for this study (Figure 1).

Figure 1 Map showing the study area of Alaska barrier islands, the four barrier islands are indicated by red arrows: Midway, Cross, Narwhal, and Stockton Islands.

2.1.1 Midway (Reindeer) Island

Reindeer Island is part of Midway Islands (beside Argo), both are low-lying areas (<1 m high) (Gibbs & Richmond, 2015). In the period from 1947 to 2006, the island migrated (on average) 329 m to the southwest in the 2000s, around 1 km to the west, split into two segments, and the total area increased from 156,010 m^2 to 352,294 m^2. From 2006 to 2010s, the island migrated around 300 m (in average), connected into one segment, increased in the spit width (Figure 2), the total area increased (almost doubled) to 711,736 m^2. The island is located about13-20 km offshore.
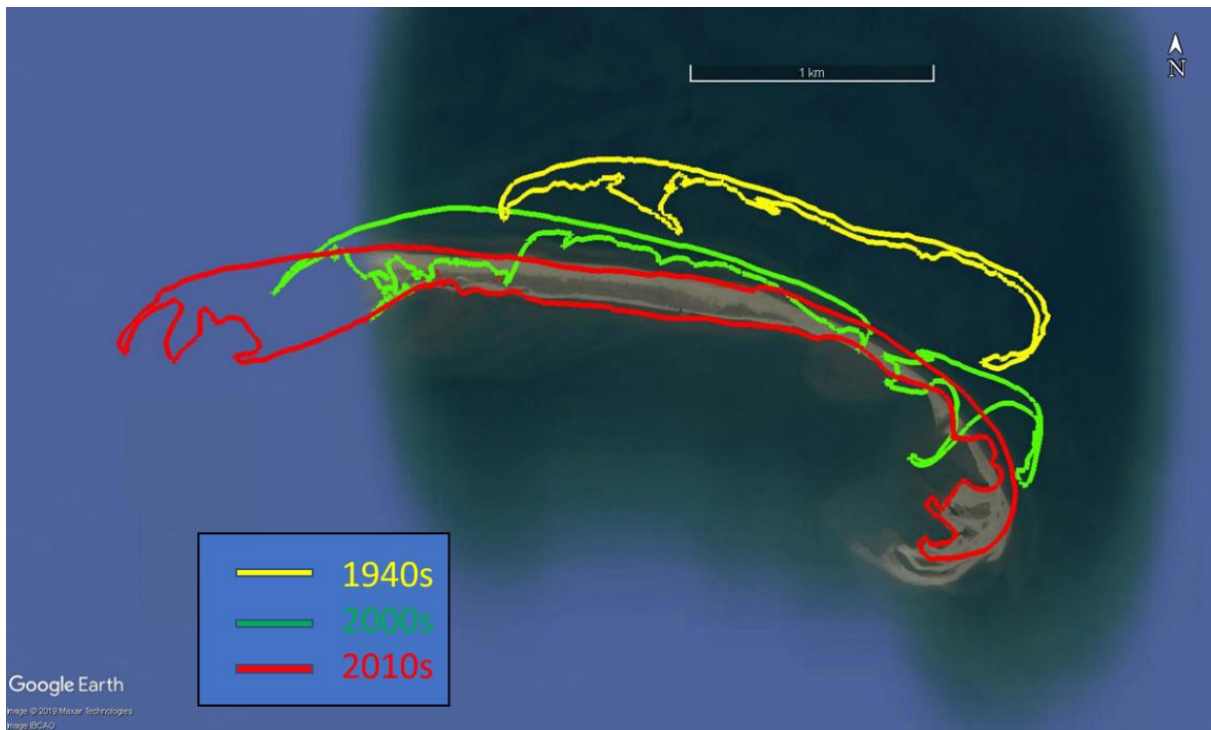
Figure 2 Historic shorelines of Midway (Reindeer) Island (shoreline data from USGS).

2.1.2   Cross Island

Cross Island is also low-lying (<2 m high) except for the constructed gravel pad part on the northwestern end (5-m high), and locates about 15 km offshore. According to an analysis by Gibbs and Richmond (2015), between 1947 and 2006, the island, merged from two separate islands (Bartlett and Cross) into one continuous island, nearly 5 km in length, and increased in area from 622.868 m^2 to $643,507 \text{ m}^2$. The southern end extended around 2 km to the southwest while the northwestern part end extended around 250 m to the west, the eastern part of the island migrated landward roughly 400 m to the southwest, in the western part, narrow spits developed over the years which lead to increase in width at that part of the island roughly from 150 m to 350m (in average).

In the period between the 2000s to 2010s, the total area increased by approximately $36,000 \text{ m}^2$, the northeastern end extended around 200m to the southwest, the middle part of the island migrated landward up to 100 m. In contrast, the southeast part almost did not migrate (Figure 3). The southern end width increased up to 160 m.
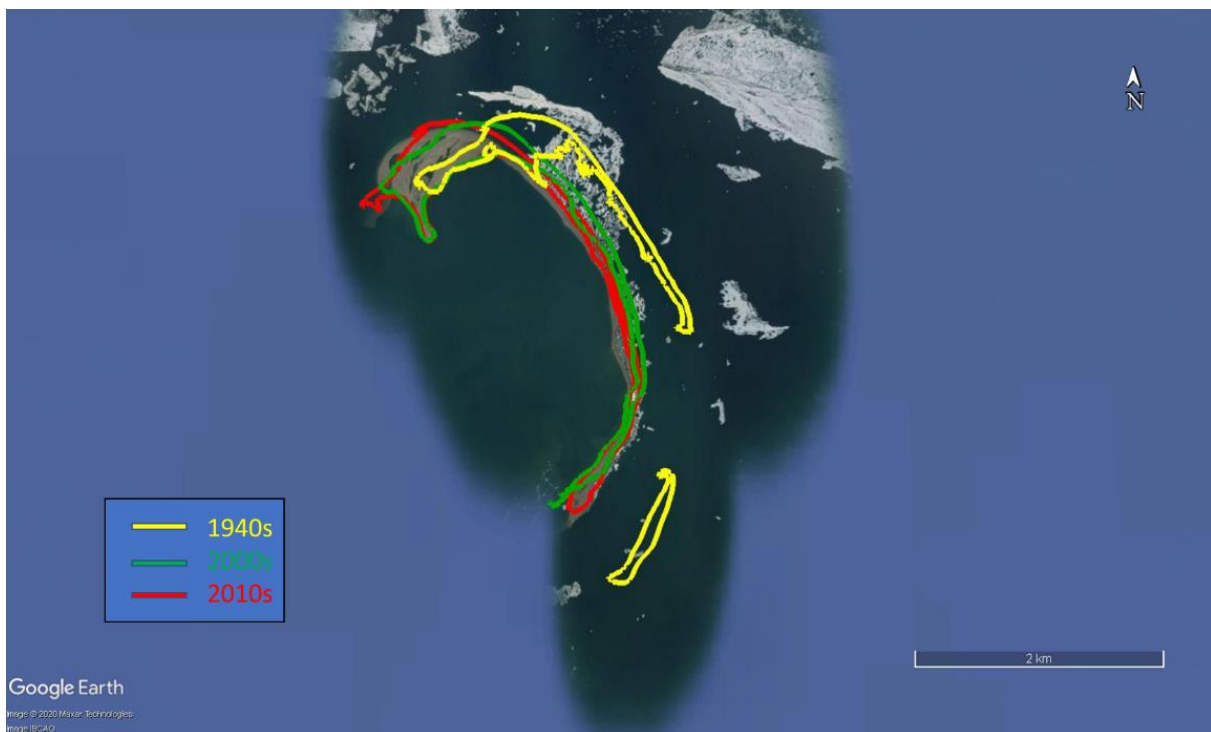
Figure 3 Historic shorelines of Cross Island (shoreline data from USGS).

2.1.3 Narwhal Island

Narwhal Island, one of McClure Islands, located at 16 km from Sagavanirktok River to the northeast. Based on the analysis by Gibbs and Richmond (2015), in the period between 1947 and 2006, Narwhal Island segmented into two separate islands. They rotated counter-clockwise, the eastern part of the island migrated landward 285 m (on average) and extended 675 m to the southwest. In comparison, the western part of the island extended about 350 m to the northwest, also extended to the southeast. In the period of 2000s to 2010s, the island segmented into 3 islands, the western part extended 500 m to the west, the middle island migrated landward with decreasing in width, the southern end extended approximately 400 m to the southwest (Figure 4).
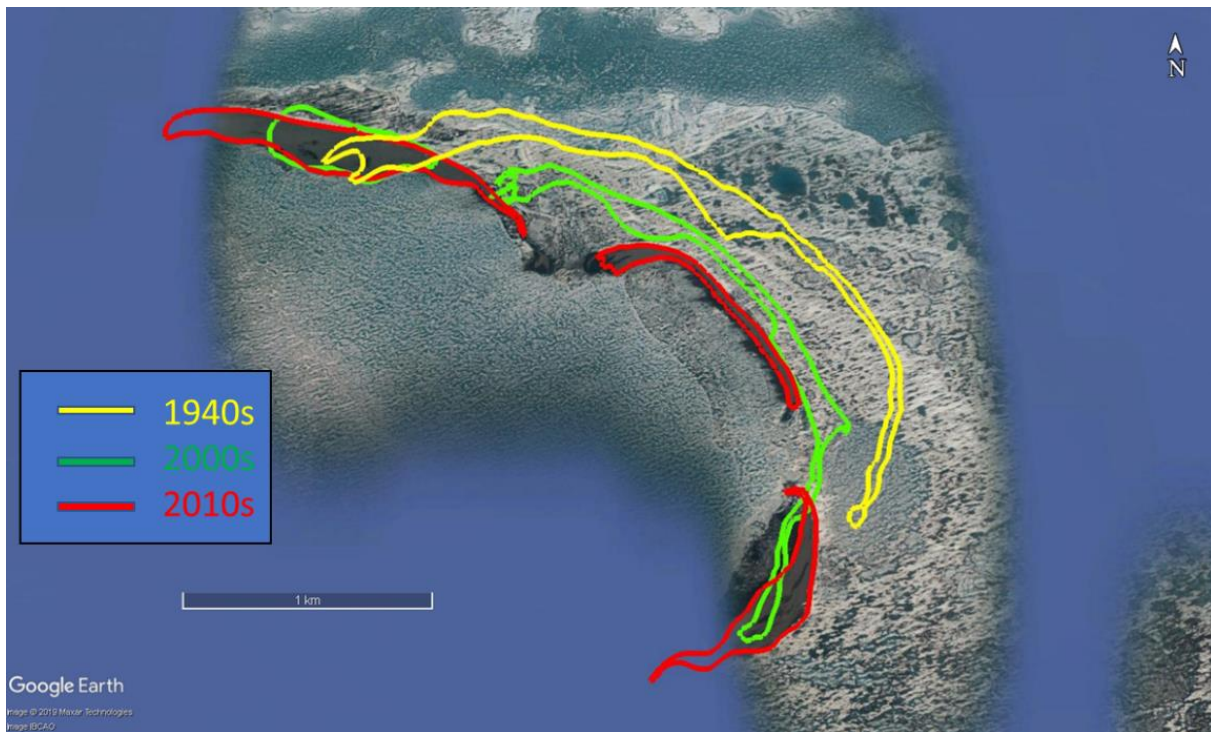
Figure 4 Historic shorelines of Narwahl Island (shoreline data from USGS).

2.1.4   Stockton Islands

The Stockton Islands, including Belvedere, Pole and numerous unnamed islands and shoals, are an approximately 8 km long (barrier chain), which are located between the so-called Challenge Entrance on the east and Newport Entrance on the west. The islands are low-lying (<2 m high).

Between the 1940s and 2000s, the Stockton Islands nearly entirely migrated landward of their 1947 position, except the central/eastern end of Pole Island did not migrate completely (Figure 5). Belvedere and Pole Islands migrated landward around 400 m and 165 m respectively, also they had merged into one nearly continuous, 8 km long island, separated by two narrow passes (Gibbs & Richmond, 2015).

Between the 1940s and 2010s, the Pole Island extended to the west around 1.5 km. The numerous small islands and shoals migrated landward and/or eroded completely.

Figure 5 Historic shorelines of Stockton Islands (shoreline data from USGS).

2.2   Data collection

2.2.1   Historical shorelines

For each barrier island, three historical shorelines were provided by USGS in the 1940s, 2000s and 2010s (Figure 2,3,4 and 5).

During the study, additional historical shorelines were extracted from satellite images using CoastSat tool (Vos et al., 2019). The shorelines were extracted from satellite images of Landsat 5, Landsat 7, Landsat 8 and Sentinel-2. The additional shorelines (Figure 6) were obtained only for Cross Island in this study to perform sensitivity tests (section 4.5).
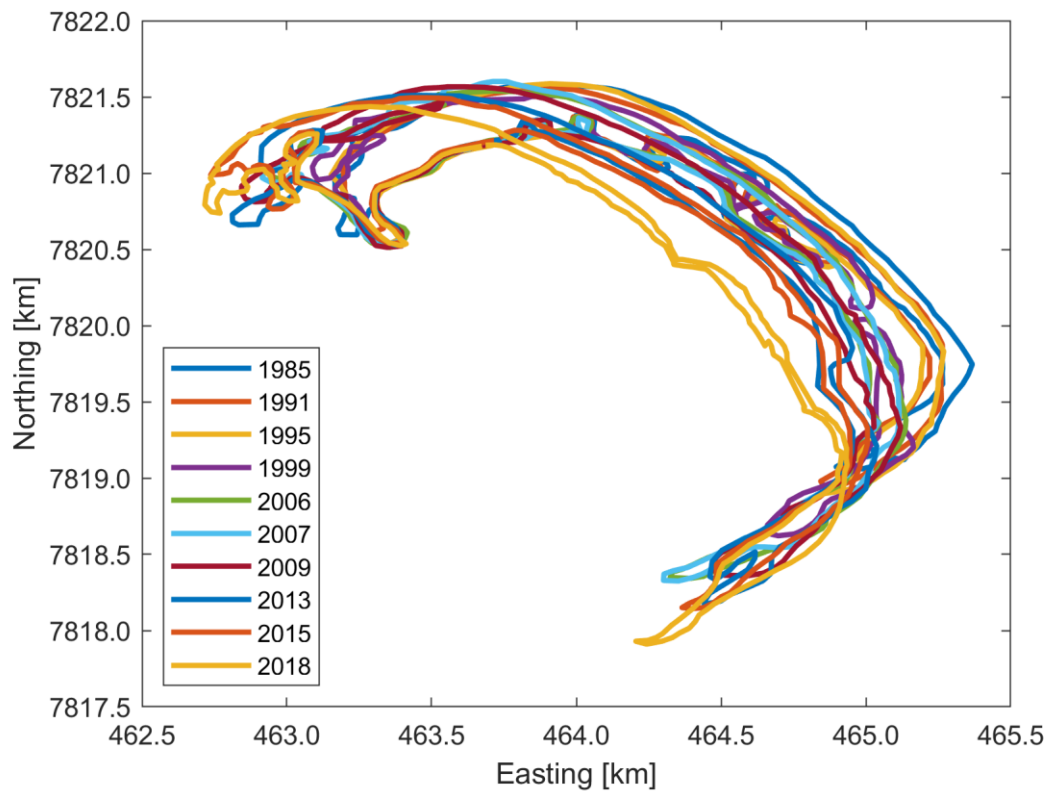
Figure 6 Historical shorelines of Cross Island extracting using CoastSat tool.

2.2.2   Wave data

The wave data used in this study is a continuous time-series of waves; the data covers the period from 1979 to 2019 (Figures 7 and 8). The data, provided by USGS, was generated with high-resolution SWAN and Delft3D models (as part of a separate project partially funded by the Bureau of Ocean and Energy Management (BOEM)).
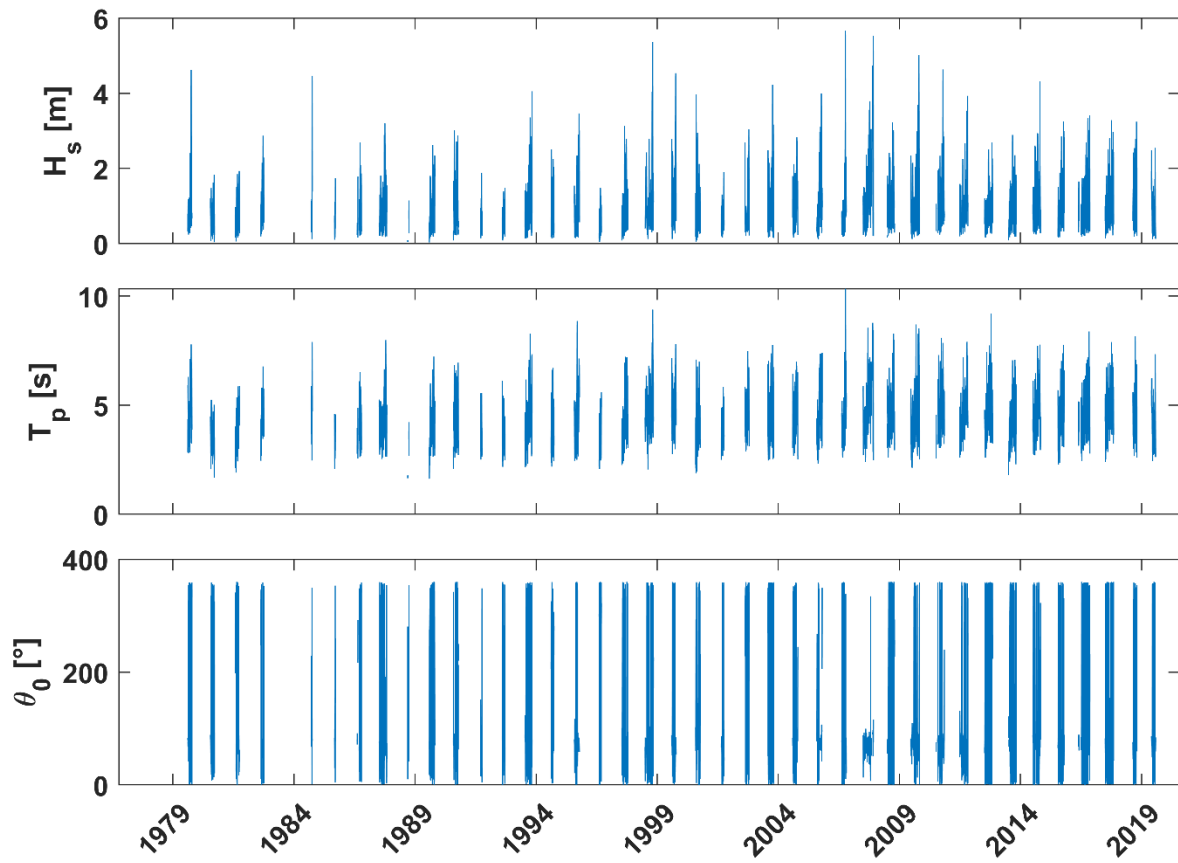
Figure 7 Time series of the wave data. H_s is the significant wave height, T_p is the peak period and θ_0 the mean wave direction.
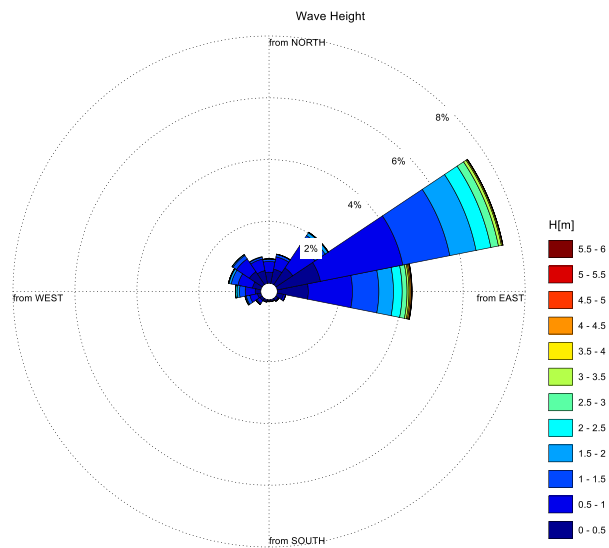
Figure 8 The wave rose shows the wave directions for the period from 1979 to 2019, and the wave height percentages

2.2.3   Bathymetry

USGS provided the bathymetry used in this study along with Delft-3D model. The bathymetry grid size is 200 m. The bathymetry domain extends from UTM (6W) Northing 7,771,516 to 7,848,477 m and Easting 4,374,897 to 5,320,220 m (Figure 9).
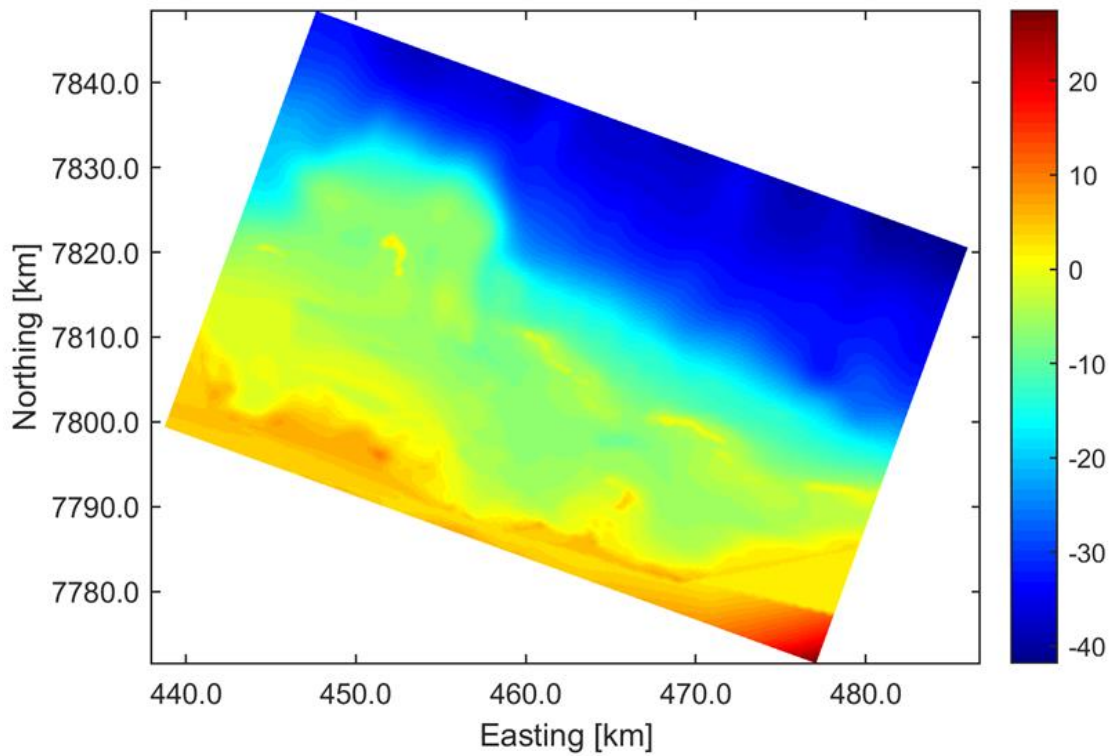
Figure 9 Bathymetry for the study area (Bathymetry data provided by USGS).

3 ShorelineS

3.1 Model description

ShorelineS is a new free-form coastline model that can describe drastic coastal transformations based on relatively simple principles of 1) alongshore transport gradient driven changes as a result of coastline curvature and 2) spit formation at high-angle wave incidence. A vector-based coastline concept is proposed, describing the coastline like a freely moving string of points. An arbitrary number of coast sections is supported, which can be open or closed and can interact with each other through relatively straightforward merging and splitting mechanisms. Rocky parts or structures may block wave energy and/or longshore sediment transport. These features allow for a rich behaviour including shoreline undulations and formation of spits, migrating islands, merging of coastal shapes, salients and tombolos.

The main formulations of the (open-source) model are presented in Roelvink et al. (2020). Test cases showed the capabilities of the flexible grid model approach. Also field validation cases for large-scale sand nourishment (the Sand Engine; 21 million m3) and an accreting groyne scheme at Al-Gamil (Egypt) show the model's capability of computing realistic rates of coastline change as well as a good representation of the shoreline shape for real situations.

3.1.1 Longshore sediment transport

In the model, the longshore sediment transport can be calculated using various formulas:

Author	Notation	Formula	
(USACE, 1984) *Introduced (Ashton & Murray, 2006)	CERC1	$Q_s = bH_{S0}^{5/2}\sin 2(\phi_{loc})$	$b = \dfrac{k\rho\sqrt{g/k}}{16(\rho_s - \rho)(1-p)}$
	CERC2*	$Q_s = K_2 H_{S0}^{\frac{12}{5}} T^{\frac{1}{5}} \cos^{\frac{6}{5}}(\phi_{loc})\sin(\phi_{loc})$	$(\phi_{loc})_i^j = \arctan 2\left(\dfrac{\sin(\phi_c - \phi_w)}{\cos(\phi_c - \phi_w)}\right)_i^j$
	CERC3	$Q_s = bH_{sb}^{5/2}\sin 2(\phi_{locb})$	$K_2 = (\dfrac{\sqrt{g\gamma}}{2\pi})^{\frac{1}{5}} K_1,\ K_1 \sim 0.4 m^{1/2}/s$ H_{sb} : Significant breaking wave height
(Kamphuis, 1992)	KAMP	$Q_s = 2.33 H_{sb}^2 T^{1.5} m_b^{0.75} D_{50}^{-0.25}\sin^{0.6}(2\phi_{locbr})$	D_{50} : median grain diameter [m] m_b : Mean bed slope (beach slope in the breaking zone) α_b : breaking wave angle

In this study the simple CERC formula was used, H_{so} is the significant wave height, b is a calibration factor and ϕ_{loc} is the local angle between representing the difference between the direction of the seaward facing shore normal and the direction of the offshore waves (both in nautical convention).

3.1.2 Wave transmission (refraction)

Although ShorelineS can simulate a range of coastline processes based on deep water wave conditions, accurate representation of the wave transformation from deep water to nearshore is required when the bathymetry is not uniform but, for instance, exhibits remnants of former deltas or eroded barriers. To this end, an efficient wave refraction solver was implemented to generate look-up tables of nearshore wave conditions as a function of location and offshore wave conditions. This stationary wave solver is generally applicable to structured and unstructured grids and has been implemented in Matlab and Fortran; implementation in XBeach and Delft3D-FM is currently undergoing testing. It has the advantage over more complex models such as SWAN that it only deals with refraction, breaking and bottom friction for directionally spread waves with a characteristic period, and is therefore much faster. Additionally, it does not suffer from the 'shadow zones' along the lateral boundaries.

The Matlab version that goes with ShorelineS produces wave conditions on a regular grid, as a function of wave height, period and direction, or a relevant subset of these, in the form of a .mat file. This can be read and interpreted by ShorelineS, which interpolates the wave conditions at points at a given distance from each shoreline point.

The wave energy balance as solved in XBeach reads:

$$\frac{\partial ee}{\partial t} + \frac{\partial ee\, C_g \cos\vartheta}{\partial x} + \frac{\partial ee\, C_g \sin\vartheta}{\partial y} + \frac{\partial ee\, C_\vartheta}{\partial \vartheta} + dd = 0 \tag{0.1}$$

where *ee* is the spectral energy density, C_g the group velocity, ϑ the wave direction and *dd* the wave dissipation density.

We can write this in simpler form:

$$\frac{\partial ee}{\partial t} + \frac{\partial ee\, C_g}{\partial s} + \frac{\partial ee\, C_\vartheta}{\partial \vartheta} + dd = 0 \tag{0.2}$$

Here, *s* is the distance along each wave direction. This can be discretized as follows:

$$\frac{ee_{k,i\vartheta}^{n+1} - ee_{ik,i\vartheta}^{n}}{\Delta t} + \frac{c_{g,k} ee_{k,i\vartheta}^{n+1} - c_{g,prev,i\vartheta} ee_{prev,i\vartheta}^{n+1}}{\Delta s_{k,i\vartheta}} + \frac{c_{\vartheta,k,i\vartheta} ee_{k,i\vartheta}^{n+1} - c_{\vartheta,k,i\vartheta-1} ee_{k,i\vartheta-1}^{n+1}}{\Delta\vartheta} + \frac{D_k}{E_k} ee_{k,i\vartheta}^{n+1} = 0,\ c_{\vartheta,k,i\vartheta} > 0$$

$$\frac{ee_{k,i\vartheta}^{n+1} - ee_{ik,i\vartheta}^{n}}{\Delta t} + \frac{c_{g,k} ee_{k,i\vartheta}^{n+1} - c_{g,prev,i\vartheta} ee_{prev,i\vartheta}^{n+1}}{\Delta s_{k,i\vartheta}} + \frac{c_{\vartheta,k,i\vartheta+1} ee_{k,i\vartheta+1}^{n+1} - c_{\vartheta,k,i\vartheta} ee_{k,i\vartheta}^{n+1}}{\Delta\vartheta} + \frac{D_k}{E_k} ee_{k,i\vartheta}^{n+1} = 0,\ c_{\vartheta,k,i\vartheta} < 0$$

$$(0.3)$$

where *k* is the grid number, $i\vartheta$ the direction bin number, *n* the timestep number, *D* the integrated dissipation, *E* the integrated wave energy. The subscript *prev* refers to the point upwind of grid point *k,* as illustrated in the figure below.
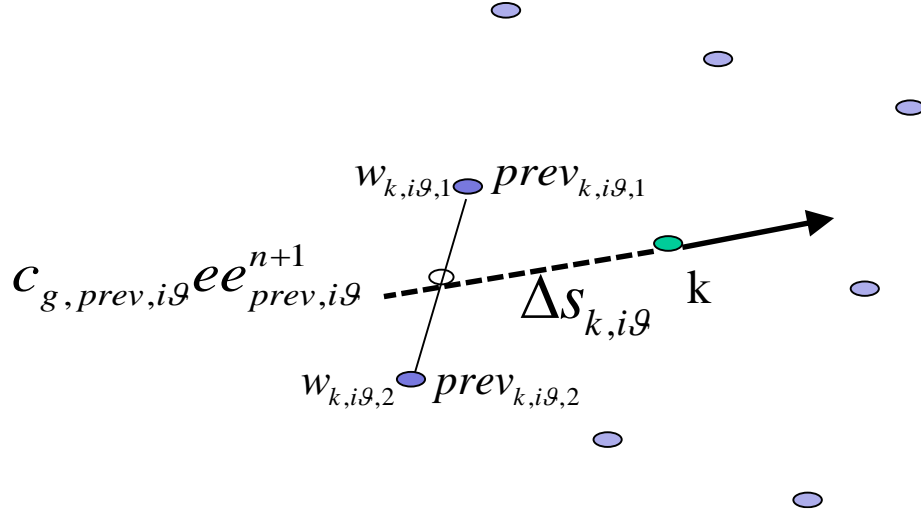
Figure 10 Stencil for the wave solver system.

We can write the system of equations per grid point as:

$$A\,ee^{n+1}_{k,i\vartheta-1} + B\,ee^{n+1}_{k,i\vartheta} + C\,ee^{n+1}_{k,i\vartheta+1} = R(ee^{n}_{k,i\vartheta}, ee^{n+1}_{prev,i\vartheta}) \tag{0.4}$$

Here, the coefficients are given by:

$$A = \frac{-c_{\vartheta k,i\vartheta-1}}{\Delta\vartheta} \quad B = \frac{1}{\Delta t} + \frac{c_{gx,}}{\Delta s_{k,i\vartheta}} + \frac{c_{\vartheta,k,i\vartheta}}{\Delta\vartheta} + \frac{D_k}{E_k} \quad C = 0 \quad R = \frac{ee^{n}_{k,i\vartheta}}{\Delta t} + \frac{c_{gx,prev}\,ee^{n+1}_{prev}}{\Delta s_{k,i\vartheta}}, \quad c_{\vartheta,k,i\vartheta} > 0$$

$$A = 0 \quad B = \frac{1}{\Delta t} + \frac{c_{gx,}}{\Delta s_{k,i\vartheta}} - \frac{c_{\vartheta,k,i\vartheta}}{\Delta\vartheta} + \frac{D_k}{E_k} \quad C = \frac{c_{\vartheta,k,i\vartheta+1}}{\Delta\vartheta} \quad R = \frac{ee^{n}_{k,i\vartheta}}{\Delta t} + \frac{c_{gx,prev}\,ee^{n+1}_{prev}}{\Delta s_{k,i\vartheta}}, \quad c_{\vartheta,k,i\vartheta} < 0$$

This is a tridiagonal system with the dimension of ntheta that can be efficiently solved for each point using a standard algorithm. The solution for each point relies on having (ideally converged) estimates of the wave energy density *ee* in the upwind points for each wave direction (Figure 10). Obviously, this works best when the points are solved after ordering by the main wave direction. Secondary effects of refraction are covered by 'sweeping' in all 4 directions. Since the wave dissipation is a very nonlinear function of the wave height and water depth the whole system needs to iteratively come to a converged solution.

3.1.3   Bathymetry update

In some coastal areas, where 2D wave solver is needed (previous section), the shoreline changes rapidly (hundreds of meter) in a short period (shorter than a decade). So updated bathymetries

are needed to provide accurate wavetable. Because of the lack of bathymetric data in many places around the world, an alternative method is needed to feed back the shoreline changes into the bathymetry. Bathymetry reconstruction from the new shoreline shape has been used in shoreline models (e.g. Kaergaard & Fredsoe, 2013; Robinet et al., 2018).

In ShorelineS, a routine was implemented to update the bathymetry at predetermined dates. The bathymetry is reconstructed using Dean profile (Dean, 1991):

$$h = Ay^{2/3}$$

where h is the water depth at a seaward distance y, and A is scale parameter depends on sediment characteristics.

First, an outer surf width should be determined based on the closure depth, and the outer surf width defines the area of the bathymetry to be updated. By using the existing grid, at each grid point within the defined area, the shortest distance to the updated shoreline is calculated, then the depth is calculated using the previous equation. For other grid points, the depths value remains the same; together, they form the updated bathymetry (Figure 11A).

When the shoreline erodes or accrete at certain parts, a (Dean) profile is created from the new shoreline position till the depth of closure. For the rest of the bathymetry (in the offshore direction) at each grid point, the depth is calculated as the minimum depth between the closure depth and the existing bathymetry (Figure 11B and C).
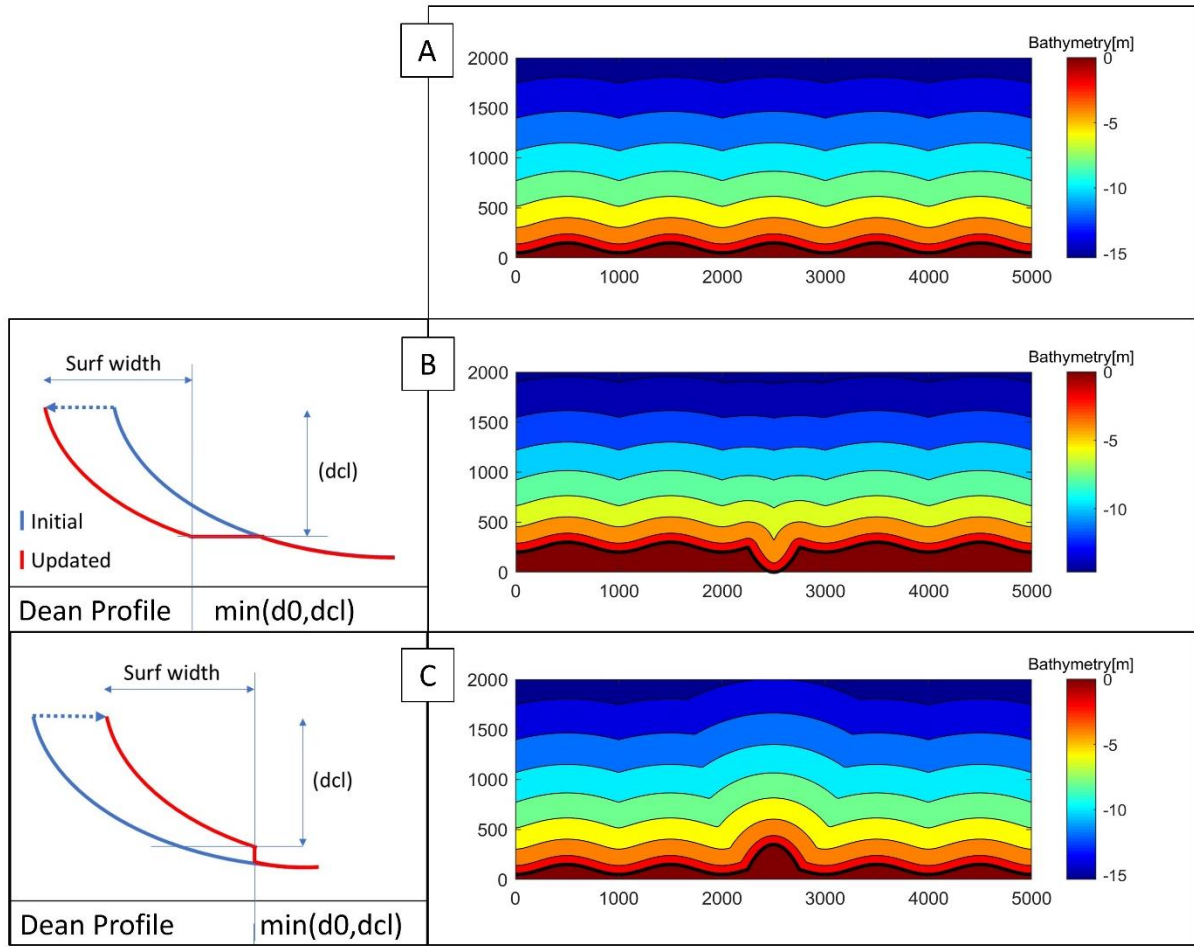
Figure 11 Mechanism of updating the bathymetry, (A) construct bathymetry from the shoreline, (B) shoreline retreat, and (C) shoreline advance.

3.1.4 Barrier rollover

In the model the barrier island rollover process is simulated using the method that was introduced by Ashton and Murray (2006), where the authors apply the critical width concept to represent the barrier overwash, so the shoreline and back-barrier positions can be calculated as follows:

$$\Delta Y_{bb} = \frac{(W_c - W_0)}{\left(1 - \frac{(D_{bb} + B)}{(D_{sf} + B)}\right)} * OWscale$$

$$\Delta Y_{sl} = \frac{(W_c - W_0)}{\left(\frac{(D_{sf} + B)}{(D_{bb} + B)} - 1\right)} * OWscale$$

14

Where ΔY_{bb} and ΔY_{sl} are the changes of the positions of the back-barrier and shoreline points respectively, W_c and W_0 are the critical width and the barrier width, B is the barrier height above the sea level, and D_{sf} and D_{bb} are the shoreface and back-barrier depths (Figure 12).
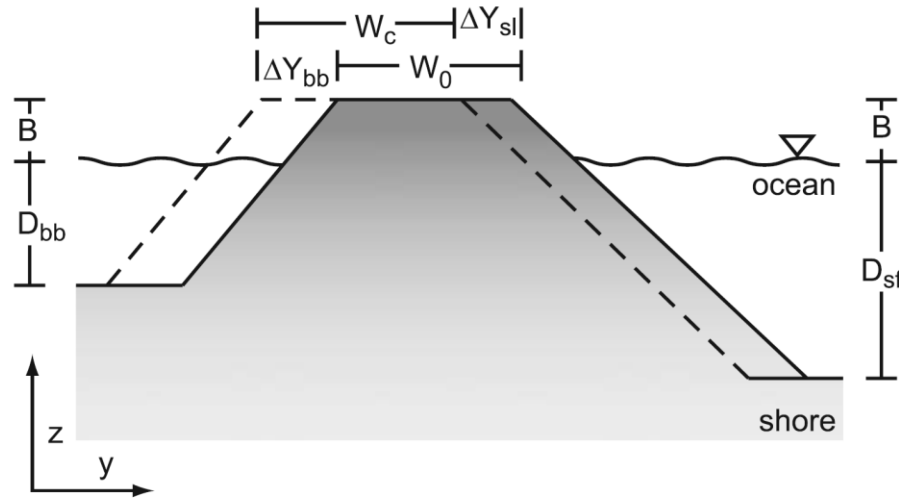
Figure 12 Schematic cross section of mass-conserving (from Ashton & Murray, 2006).

In the previous equations, the term *OWscale* was added to the original equation as a calibration factor in the model. The reason behind adding such a factor is that the rollover occurs on the long time scale (e.g. years), However, the routine works every time step (in a scale of hours or days), so the rollover distance should be reduced by a factor which is *OWscale*.

3.1.5   Upwind correction

To avoid unstable behavior, or not to underestimate for the spit growing in ShorelineS, an upwind correction was implemented. Which is a special treatment takes care of so-called high-angle instability (Ashton et al., 2001), such instability happens when a grid point experiences high-angle waves but its updrift adjacent point experiences low-angle waves or the opposite. The are several methods to apply the upwind correction; in this study, two methods were tested:

1. First method

The adjacent segment down drift receives half of the maximum angle flux; then the next segment flux is zero; also the updrift segment receives half of the maximum angle flux, and the flux of segment before it receives zero (Figure 13-A).

2. Second method

The adjacent segment flux down drift receives at least half of the maximum angle flux then the next segment receives at least zero, while the updrift segment receives at least maximum half of the segment flux and the flux does not exceed zero for the segment (Figure 13-B).

15
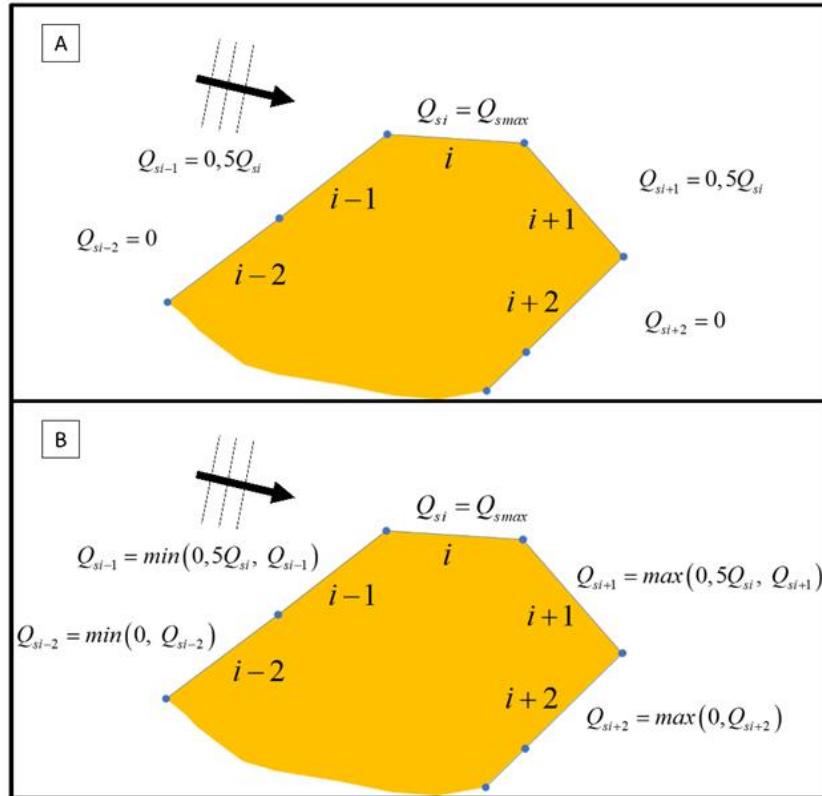
Figure 13 schematization of the upwind correction applied in the model (a) first method, and (b) second method.

3.2 Model setup/parameters

In this section, the input parameters is explained.

3.2.1 Wave conditions

The wave conditions could be introduced in ShorelineS in three different approaches:

3.2.1.1 Time series file

The time series wave data were obtained at an interval of 1 hr, and to avoid long simulation running time, the wave data were re-computed at an interval of 24 hr using the following formulas:

$$H_{s,24h} = \sqrt[2.5]{\frac{\sum_{i=1}^{n} H_{s,1h}^{2.5}}{24}}$$

$$T_{p,24h} = \frac{\sum_{i=1}^{n}\left(H_{s,1h}^2 \cdot T_{p,1h}\right)}{\sum_{i=1}^{n}\left(H_{s,1h}^2\right)}$$

$$\theta_{m,24h} = \arctan 2\left(\frac{\sum_{i=1}^{n}(H_{s,1h}^{2.5} \cdot \sin\theta_{m,1h})}{\sum_{i=1}^{n}(H_{s,1h}^{2.5} \cdot \cos\theta_{m,1h})}\right)$$

Where $H_{s,1h}$, $T_{p,1h}$, and $\theta_{m,1h}$ are the original wave conditions (with 1hr interval), and $H_{s,24h}$, $T_{p,24h}$, and $\theta_{m,24h}$ are the representative wave conditions (with 24 hr interval).

3.2.1.2   Wave climate schematization

In order to speed up the simulations, one approach is to reduce the number of time steps needed to run the model. Since the model using adaptive time step, a number of wave conditions that represent the wave data could be selected, and then the model calculates the maximum suitable time step. The determination of the representative wave conditions is called wave climate schematization.

Different methods to schematize the wave climate were introduced in Benedet et al. (2016). In this study, the energy flux method is used. In this method, the user defines the number of directional bins (intervals) and wave height bins. In this study, the numbers of bins selected are 8 and 3, respectively.

For the calculations, first, the wave energy flux is calculated for all the wave record, using the following equation:

$$E_f = \frac{\rho g H_s^2}{8} C_g$$

Where ρ is the water density, g is the gravity acceleration, and C_g is the group wave celerity, in deep water.

Second, as depicted in Figure 14, the (8) directional bins' outlines are calculated as 'equal wave energy' bins. Then each directional bins divided in (3) wave height bins using same energy concept, so all the final wave (24) classes have the same total wave energy flux (Figure 14). Each time step, a wave condition is selected randomly from these 24 conditions.
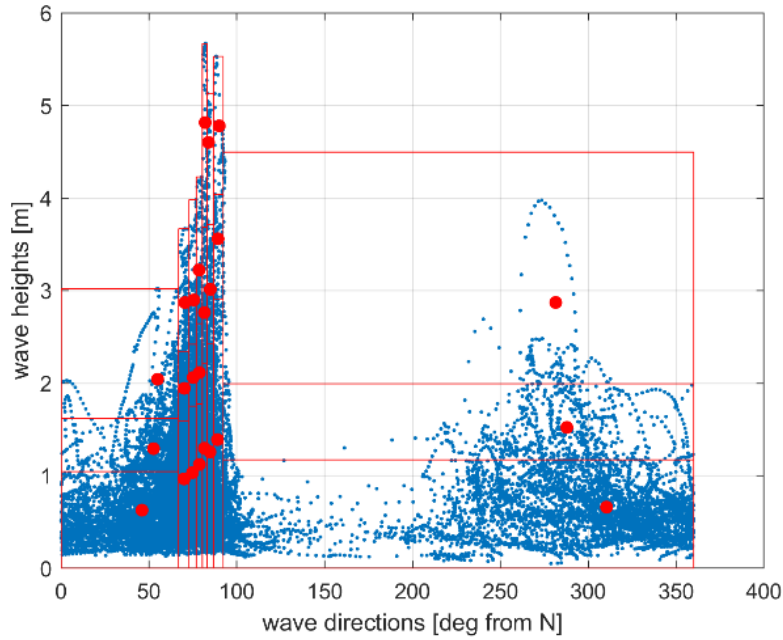
Figure 14 Wave climate based on the provided wave data, all wave records (blue dots), wave bins' class (red rectangular) and representative of wave bins (red dots).

3.2.1.3   Mean wave direction

The third approach to define the wave conditions is by using one value for wave direction, which is the long-term average wave direction; also a random spreading over a sector of certain degrees around the mean could be added. The random spreading is preferred to avoid instabilities due to high wave angles, which is reduced in reality as the effect of local refraction. Also, one value for the wave height represents the long term wave height.

3.2.2   Closure depth and Surf width

The depth of closure is playing an essential role in the model; as it controls the shoreline displacement through the longshore transport formula, also it controls updating the bathymetry when needed (section 3.1.3). Following a study by Brutsché et al. (2014), that presented several methods to calculate the depth of closure, as follows:

- Equations by Hallermeier (1981)

$$d_l = 2.28 H_e - 68.5(\frac{H_e^2}{gT_e^2})$$

$$d_l = 2\overline{H_s} + 11\sigma_s$$

- Equations by Birkemeier (1985)

18

$$d_l = 1.75H_e - 57.9(\frac{H_e^2}{gT_e^2})$$

$$d_l = 1.57H_e$$

Where H_e is the effective wave height or wave conditions that exceeded only 12 hours out of a single year, T_e is the associated wave period, $\overline{H_s}$ is the annual mean significant wave height, and σ_s is the associated standard deviation of the significant wave height.

For the previous equations, there are two methods to calculate H_e, either as

$$H_e = \overline{H_s} + 5.6\sigma_s$$

or as the top 0.137% wave height in a year, the two methods used with the three questions above (6 methods), in addition to the second equation so there are seven different methods. The seven methods were used to calculate the depth of closure based on the wave data for every year; then, the maximum value was calculated (Figure 15).
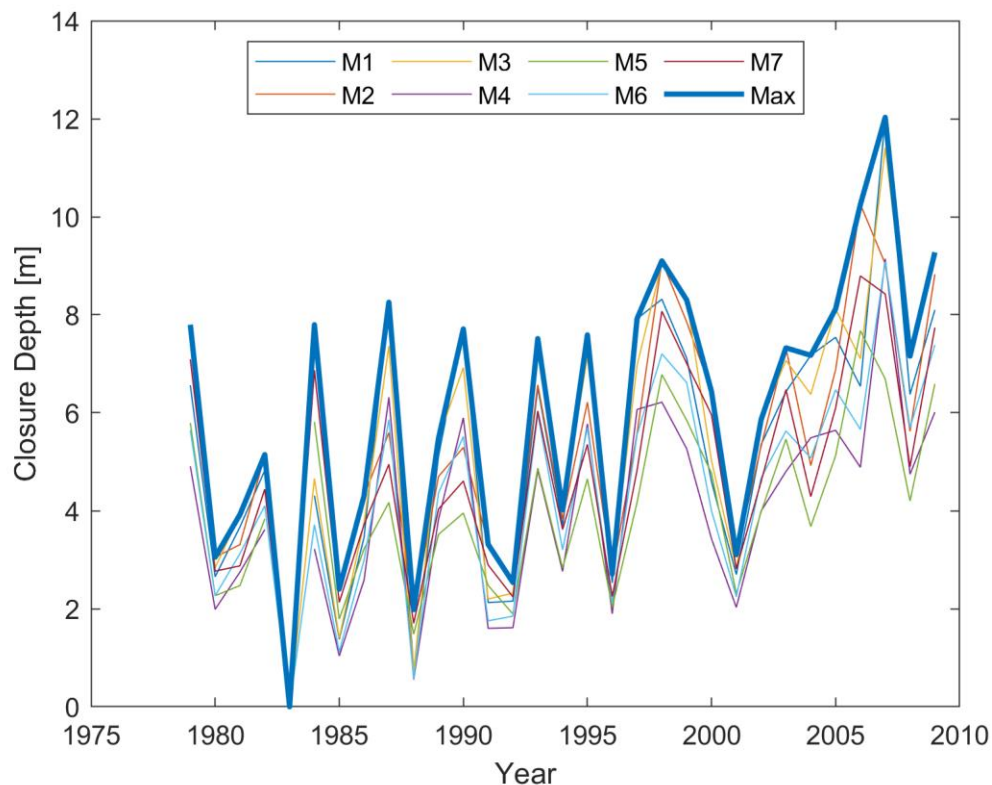
Figure 15 The depth of closure calculation using seven different methods and the maximum values every year (blue line).

As shown, the calculated depth range is changing between 2 and 8 m, except in 2007 due to the higher wave conditions, the estimated depth equals to 12 m.

Based on the depth calculations, the surf widths were estimated using Dean profile, then were sorted in descending order (Figure 16). For the dominant closure depths, the surf widths are ranging between 250 to 1000 m.
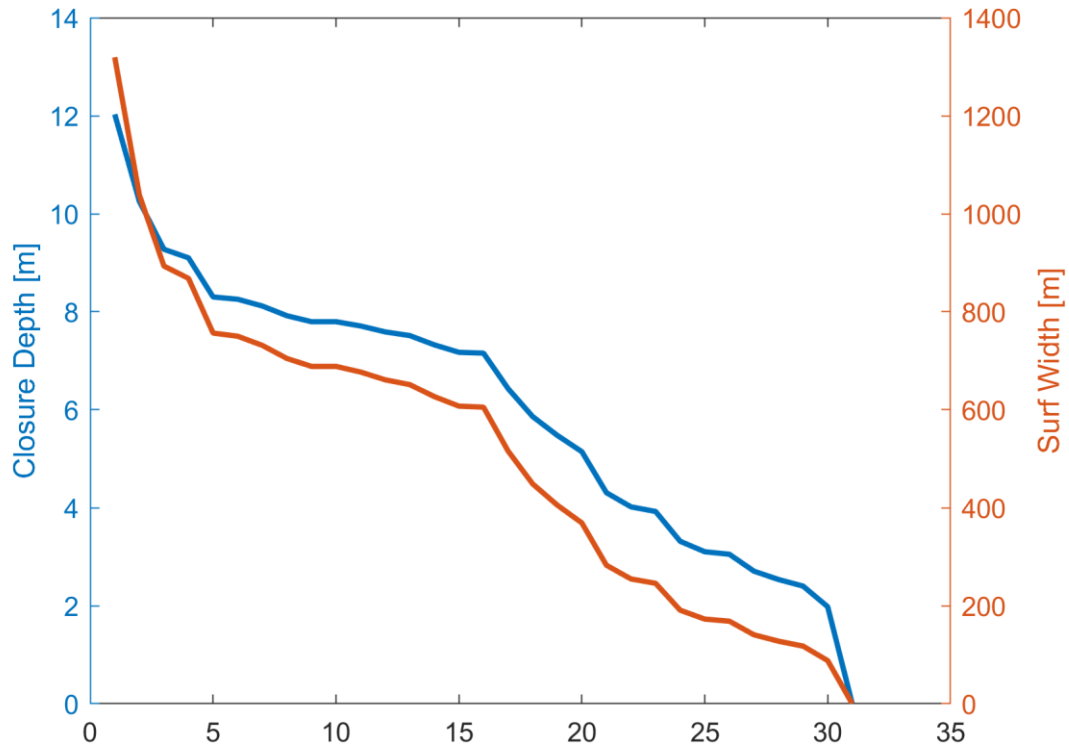
Figure 16 The estimated surf width (orange) and closure depth (blue) based on the wave data, the values are in descending order.

3.2.3   Barrier island configuration

The barrier configuration parameters such as barrier width, barrier height, shoreface and back-barrier depths are needed in the model (section 3.1.4). To better estimate the parameters' values, cross sections were extracted from the available bathymetry data (Figure 17). The barrier heights values were ranged between 0 to 1.5 m.
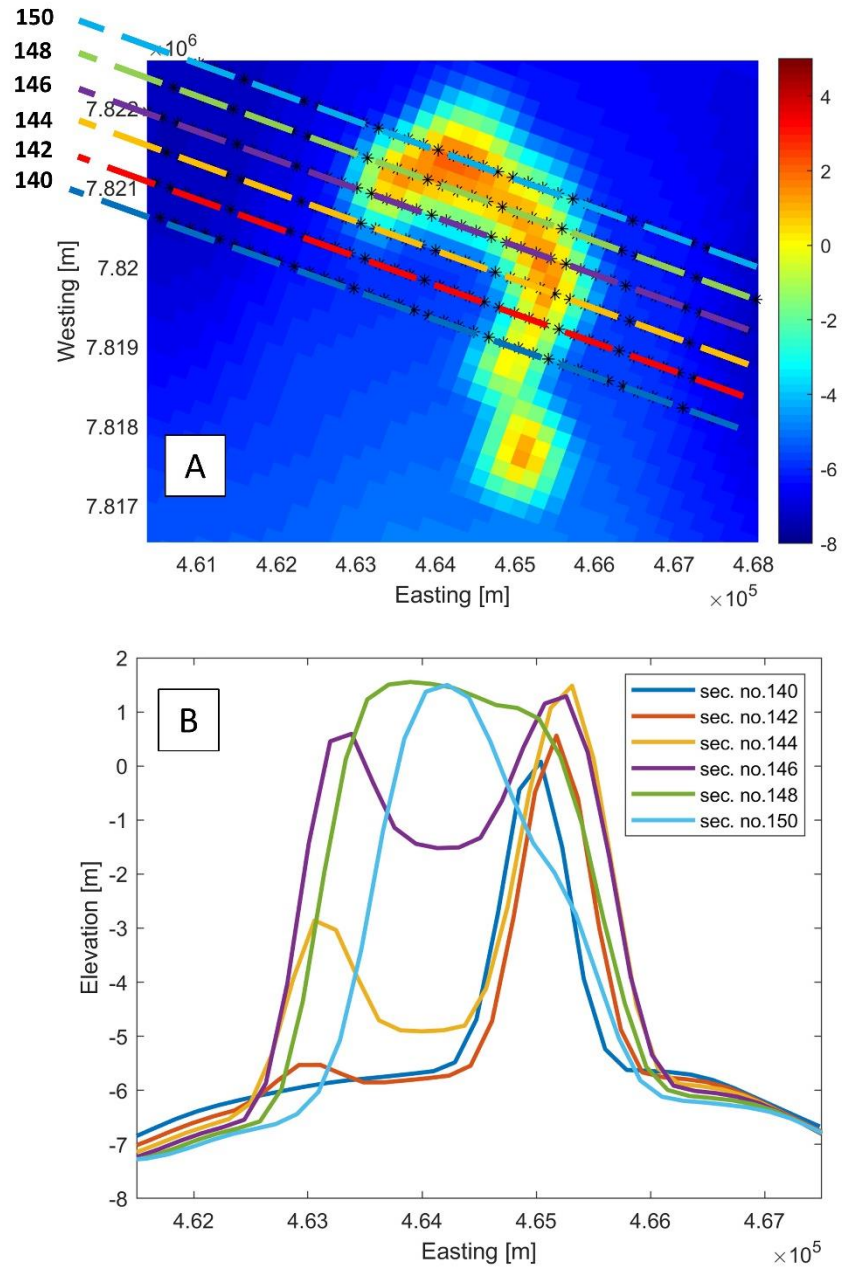
Figure 17 Cross shore profiles along Cross Island barrier, (a) cross section positions on top of the bathymetry, and (b) the cross sections.

3.2.4 Model parameters

Based on the formulations presented in the previous sections, 13 parameters were chosen to calibrate the model and to study the model sensitivity to each of them. In Table 3-1, the parameters are presented, for each parameter range of values were determined based on the available data and previous user experience.

Table 3-1 Model calibration parameters

Parameter	Values		
Depth of closure (D_c) [m]	5	10	15
Surf width [m]	500	200	100
Barrier height (BH) [m]	1	1,5	
Spit width [m]	200	250	300
Smooth factor	0,1	0,05	0,01
LT equation	CERC	CERC2	KAMP
LT coeff. (b)	0,1 e6	0,3 e6	0,5 e6
Grid size (ds) [m]	25	50	100
Two points	1	2	
Surfwidth$_i$ [m]	100	200	300
Surfwidth$_o$ [m]	300	500	1000
Owscale	0,0001	0,0005	0,001
Active for shoreface & back-barrier	equal	varied	

For the longshore sediment transport calculations, the type of equation and the coefficient b are controlling the process. Although the depth of closure effect can be presented in b, it was chosen to be calibrated as it affects the barrier rollover process as well, in addition to barrier height, OWscale, spit width and back-barrier depth. The latter value could be equal to or less than shoreface depth, which assumed to be equal to the depth of closure.

A certain amount of smoothing (smooth Factor) is applied in order to minimize variations in grid size during the regridding, which has to occur constantly because of the spit migration. However, this can lead to sediment loss and should be maintained as low as possible.

The "two points" parameter represents the upwind correction approaches, as discussed in section 3.1.5.

Surfwidth$_i$ is the inner surf width where the model interpolates the alongshore-varying wave directions and heights to use in the transport formula (section 3.1.2), while Surfwidth$_o$ is the outer surf width that bounds the updated area of the bathymetry.

3.3   Model performance evaluation

In this section, the approaches to evaluate the model performance are presented.

3.3.1   Brier Skill Score

The Brier Skill Score (BSS), which is commonly used to evaluate the morphological model results (e.g. van Rijn et al., 2003; Sutherland et al., 2004), was used in this study. The BSS is calculated as follows:

$$BSS(t) = 1 - \frac{rmscm(t)}{rmsm(t)}$$

Where $rmscm(t)$ is the root mean square of the difference between the measured and computed coastlines, and $rmsm(t)$ is the root mean score deviation of the measured coastline at any specific time (t), they are calculated as:

$$rmscm(t) = \sqrt{\frac{1}{L} \int_{0}^{L} dist_{comp(t)-meas(t)}^{2} \, ds}$$

$$rmsm(t) = \sqrt{\frac{1}{L} \int_{0}^{L} dist_{meas(t)-initial}^{2} \, ds}$$

Where $dist_{meas(t)-initial}$ are the minimum distances between the measured and the initial coastlines, $dist_{comp(t)-meas(t)}$ are minimum the distances between the computed and the measured coastline, ds represent the coastline segments based on the model discretization, and L is the total length of the coastline segments.

For using BSS, van Rijn et al. (2003) proposed qualifications for the morphological models' performance (Table 3-2).

Table 3-2 Qualification for morphological models performance

Qualification	BSS
Excellent	0.8-1.0
Good	0.6-0.8
Reasonable/fair	0.3-0.6
Poor	0-0.3
Bad	<0

3.3.2   Total land area

One of the challenges to simulate (very dynamic) barrier islands using a one line model is the total land area. As shown in the next chapter, the land areas are changing rapidly over the years.

So the computed land areas to the measured were used as a second criterion to evaluate the model performance.

4 Results and discussion

The previous parameters were tested in two phases; first, all mentioned parameters were tested with Cross Island, then a narrower range of values were chosen to be applied with the other islands based on the preliminary tests. Second, a reduced range of values was selected to be tested for a shorter period to test the sensitivity of the model (section 4.5).

For the first phase, the shorelines provided by USGS were used in a simulation period from 2000 to 2010; however, the dates of the shorelines were not accurately determined. For the second phase, the shorelines extracted by CoastSat (Figure 6) were used.

In the following sections, the inputs of the successful simulations are presented (Tables 4-1, 2, 3, 4, and 5), and selected results are presented. The failed simulations are not presented but will be discussed.

For the wave conditions, the three possible options (section 3.2.1) were tried with a different set of other parameters; however, the time series resulted in more reasonable result, in the following presented simulations the wave series were used as input.

For updating the bathymetries different values for the outer surf width were tested, in the following simulations, a 1000 m was used.

4.1 Cross Island

The Cross Island was chosen to start the model testing because it is less complex than the other islands, all the values for the parameters discussed in chapter 3 were tested. In Table 4-1 few results are presented; however, all the lessons learned will be mentioned.

Table 4-1 Cross Island simulation trials using USGS shorelines

	Bathymetry update	Surfwidth$_i$	D_c	OWscale	BH	ds	Spit width	BSS	Total Area
1	5 years	250	10	0,001	1,5	50	250	0,2519	601272
2	5 years	350	10	0,001	1,5	50	250	0,34339	598510
3	2 years	250	10	0,001	1,5	50	250	0,08396	605983
4	5 years	250	10	0,0005	1,5	50	250	0,17595	600087
5	5years	250	10	0,001	1,5	50	250	-0,2056	598789
6	5 years	250	7	0,001	1,5	50	250	0,37891	598399
7	5 years	150	10	0,001	1,5	50	250	-	
8	5 years	250	10	0,001	1,5	50	300	0,18524	598900
9	5 years	250	10	0,001	1	50	250	0,01881	590636
10	No	250	10	0,001	1,5	50	250	0,0890	600722
11	5 years	250	8,5	0,001	1,5	50	250	0,2066	593382
12	5 years	300	10	0,001	1,5	50	250	0,3829	605242
13	5 years	250	10	0,001	1,5	25	250	-4,4893	-
14	5 years	300	8,5	0,001	1,5	50	250	0,2812	589744

15	5 years	250	10	0,001	1,5	50	250	-	
16	5 years	300	10	0,001	1	50	250	-0,2355	590180
17	5 years	300	8	0,001	1,5	50	250	0,1676	589764
18	5 years	250	10	0,0005	1,5	50	250	-1,8431	647955
19	5 years	0	8,5	0,001	1,5	50	250	0,3407	589245
20	5 years	300	10	0,0001	1	50	250	0,40917	605045
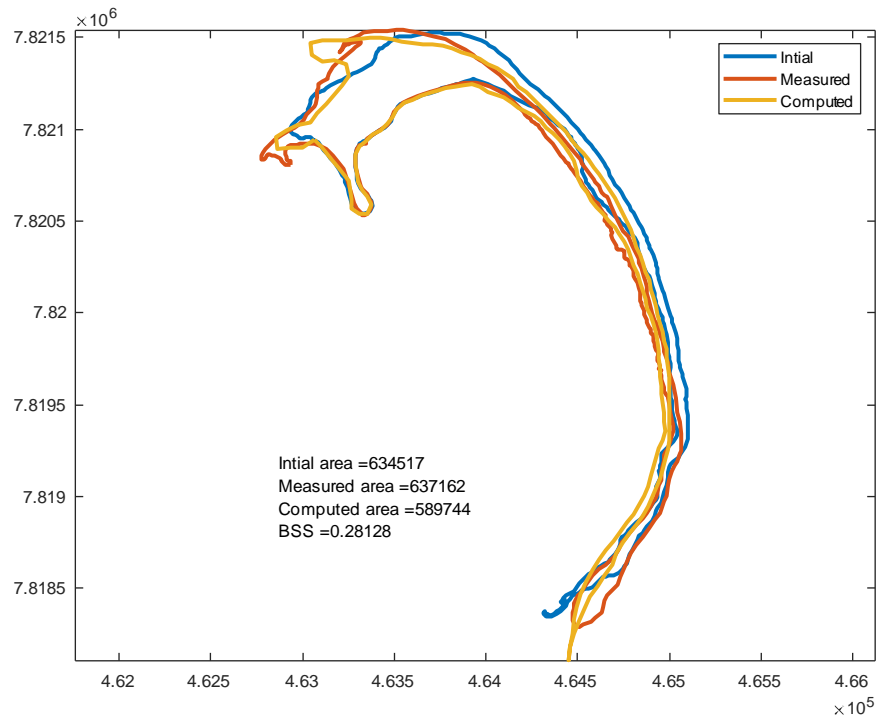
Figure 18 Cross Island, result no. 14, initial shoreline (blue) at 2000, measured (red) and computed (yellow) at 2010.
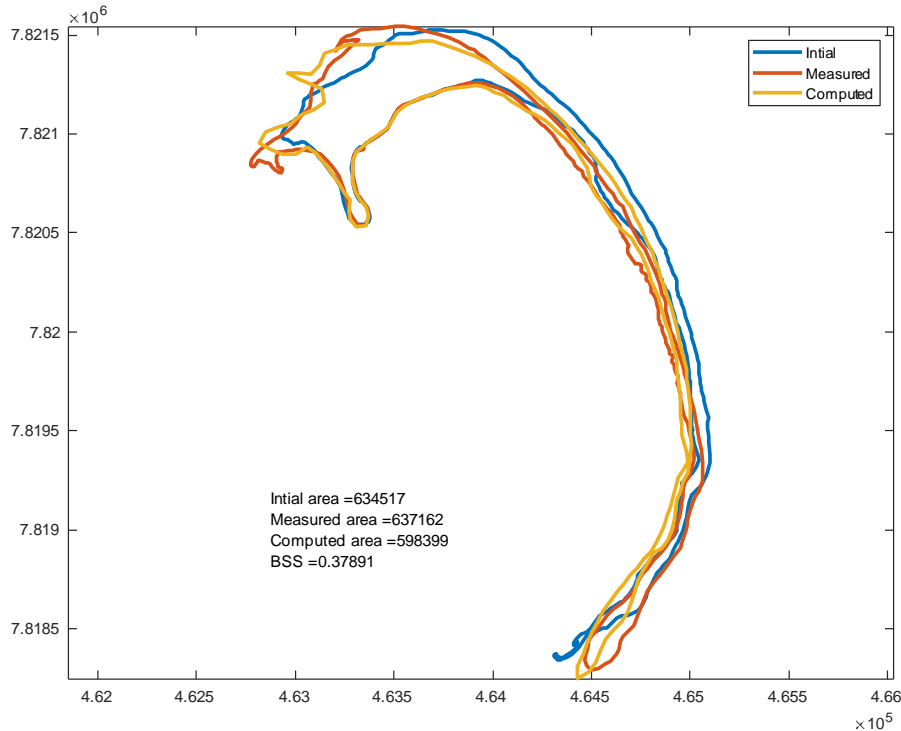
Figure 19 Cross Island, result no. 6, initial shoreline (blue) at 2000, measured (red) and computed (yellow) at 2010.

Overall, the results showed that the highest value for BSS was around 0.4, which consider fair according to the evaluation criteria. For the total computed area, the average difference in the reasonable simulations around 30000 m^2.

The barrier rollover process that was happening at the middle to the southern part of the island was well-simulated, after tuning the OWscale to the values presented in the tables. The northwestern part where the spit should extend to the west, such behavior, the model was able to simulate in several simulations. However, the northern part, where layers of thin spits grow over the years, the model was not able to reproduce the spit growing in the right direction.

4.2   Reindeer-Midway Island

For this island, it is clear from the initial and the measured area that total area was increased by a factor of two. In order to increase the total area, based on the rollover formula (section 3.1.4), a different value for shoreface depth and back-barrier depth were used. A fixed value for the depth of closure 10 m was used. The other parameters are mentioned in Table 4-2.

Table 4-2 Reindeer-Midway Island simulation trials using USGS shorelines

	bathymetry update	surf width	OWscale	BH	spit width	b [10^6]	Dsf	Dbb	BSS	Total Area
1	1 year	300	0,0001	1	300	0,3	8	4	-0,333	661419

27

2	2 years	300	0,0001	1	300	0,3	8	4	-0,296	695162
3	2 years	300	0,0001	1	300	0,3	8	4	0,062	568432
4	5 years	300	0,0001	1	300	0,1	10	10	failed	
5	5 years	150	0,001	1,5	250	0,1	10	10	-0,621	238604
6	2 years	150	0,0001	1,5	250	0,1	8	6	-0,058	327825
7	2 years	150	0,0001	1,5	350	0,3	8	4	-0,446	730221
8	2 years	150	0,0001	1,5	350	0,1	8	4	0,073	532346
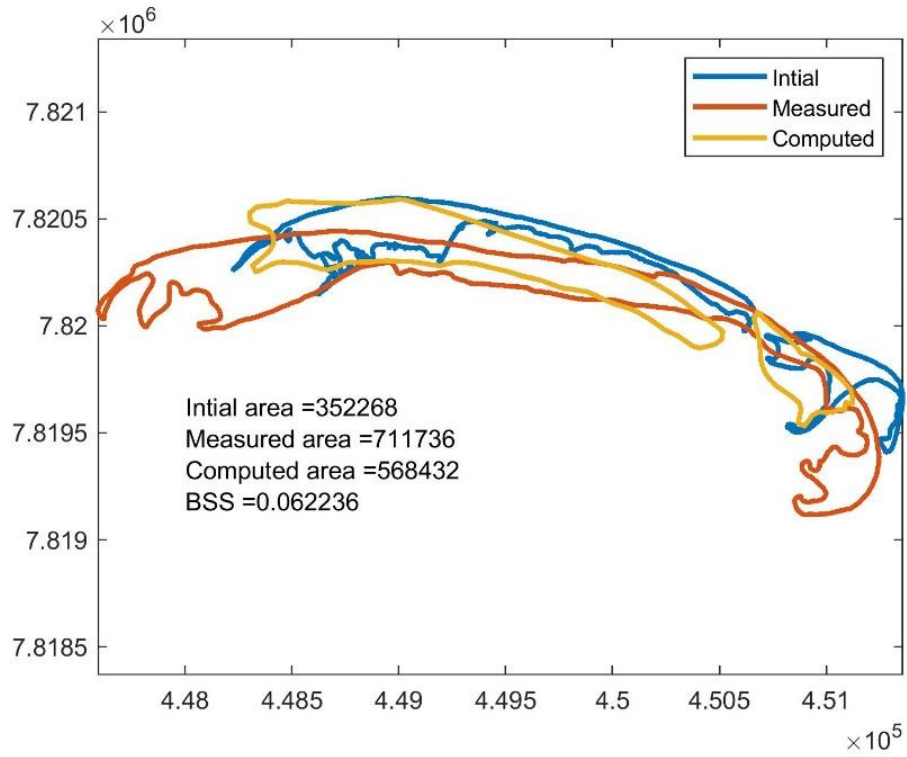
Figure 20 Reindeer-Midway Island, result no.3 , initial shoreline (blue) at 2000, measured (red) and computed (yellow) at 2010.
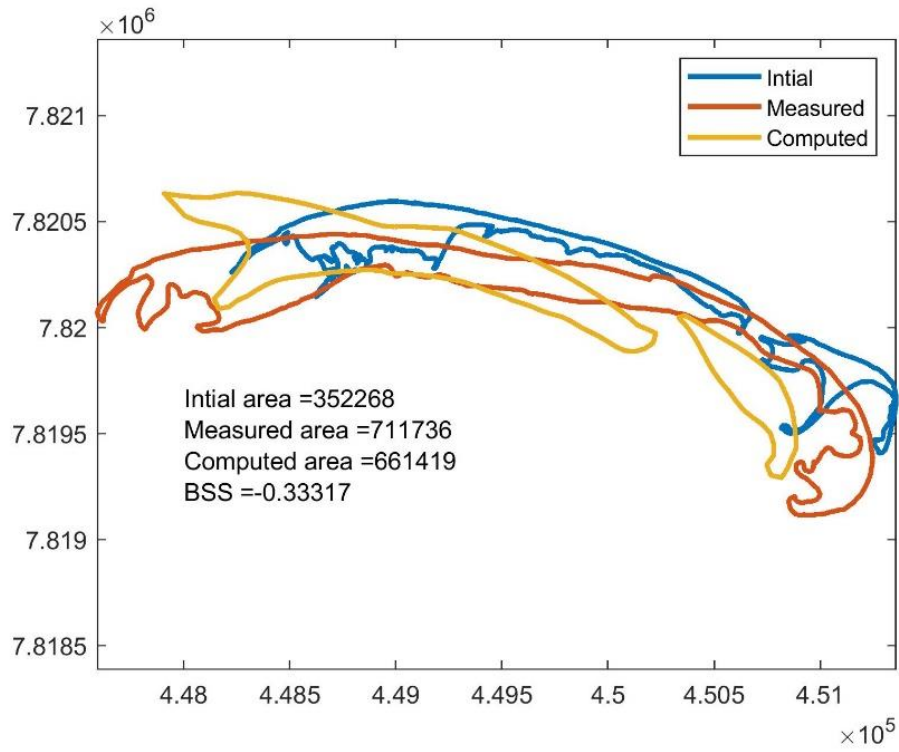
Figure 21 Reindeer-Midway Island, result no. 1, initial shoreline (blue) at 2000 , measured (red) and computed (yellow) at 2010.
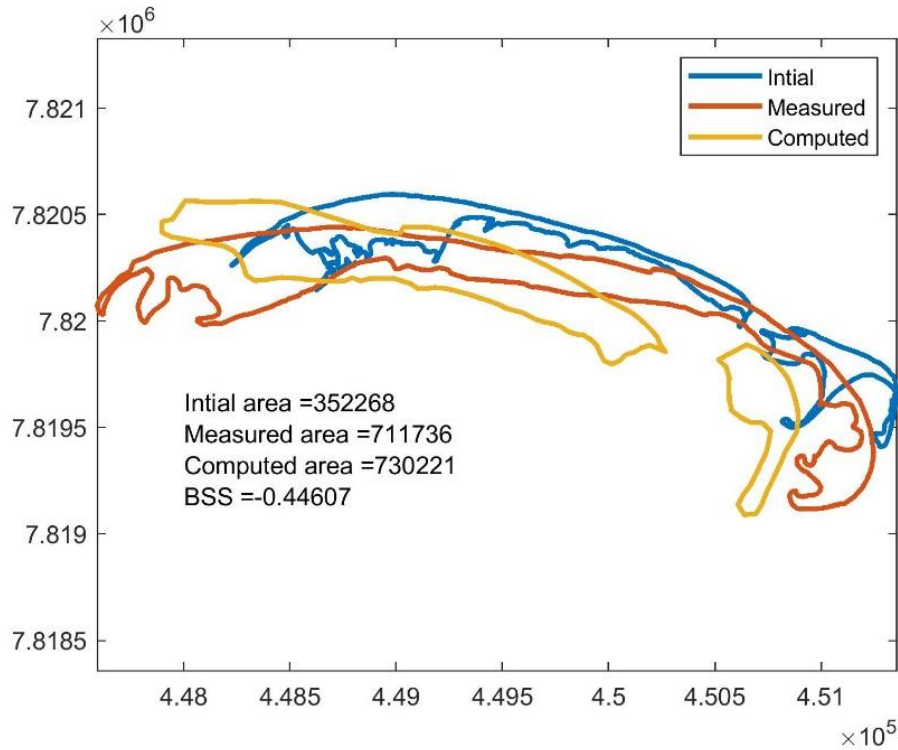
Figure 22 Reindeer-Midway Island, result no. 6, initial shoreline (blue) at 2000 , measured (red) and computed (yellow) at 2010.

As shown in the previous figures, three main processes that happened to the island within the simulated period should be observed in the model:

- first, the two parts of the island were merged, in all the simulations the island two parts never merged; however, they get very close at the beginning.
- Second, the middle part of the island is migrating toward the south; also, the surface area is increasing, the model was able to increase the surface area, but the overall direction is not matching.
- Third, the western part is growing to the west direction; the model was able to reproduce; however, not in the right direction (Figure 21 and **Error! Reference source not found.**).

4.3   Narwhal Islands

In Narwhal Islands, the behavior is more complicated. Based on the experience from the two previous islands, fewer simulations were made; also, several simulations failed to be completed, in Table 4-3 three results are presented.

Table 4-3 Narwhal Islands simulation trials using USGS shorelines

	bathymetry update	surf width	closure depth	OWscale	barrier height	spit width
1	5 years	300	8,5	0,0001	1	250
2	5 years	300	8,5	0,00001	1	250

| 3 | 5 years | 300 | 12 | 0,0001 | 1 | 250 |
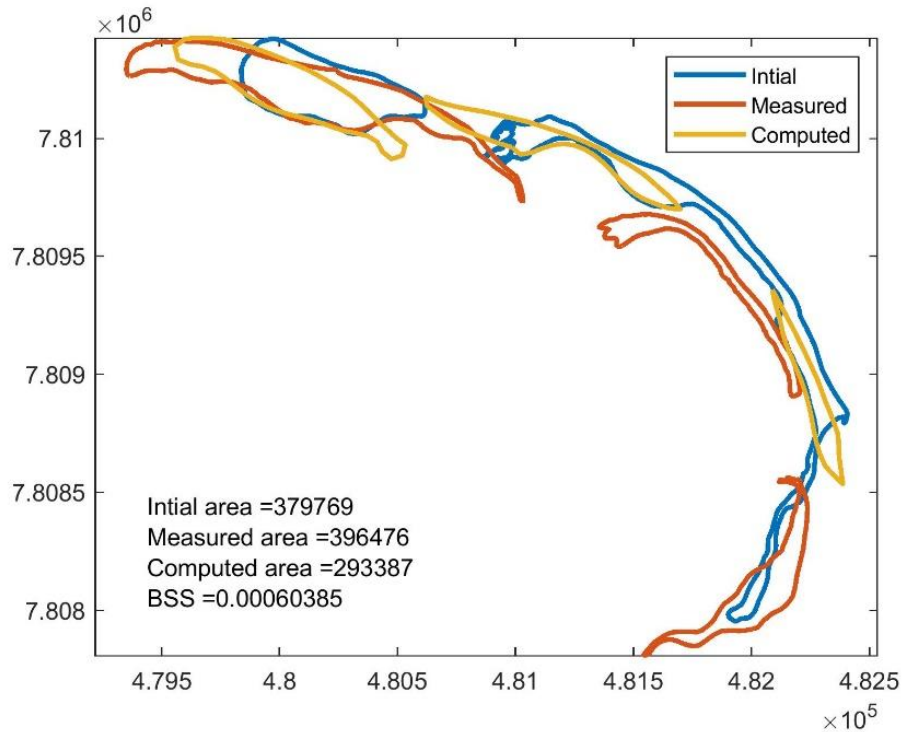
Figure 23 Narwahl Islands, result no. 2, initial shoreline (blue) at 2000, measured (red) and computed (yellow) at 2010.

As shown in the previous figure, the southern island should be split into two parts; one was reduced in area, and the other migrated and grew southward, in the model, the very southern area disappeared while the middle-upper part extended to the northwest. The northern island should extend to the east and the west, which the model did but not in the right direction.

4.4   Stockton-Pole Islands

The Stockton-Pole Islands are complex; however, were given few trials, in Table 4-4, two simulation inputs are presented. The values of BSS do not reflect the performance of the model for these islands.

Table 4-4 Stockton-Pole Islands simulation trials using USGS shorelines

	bathymetry update	surf width	closure depth	OWscale	spit width	b [10^6]
1	5 years	300	10	0,0001	250	0,1
2	5 years	250	8,5	0,0001	250	0,3
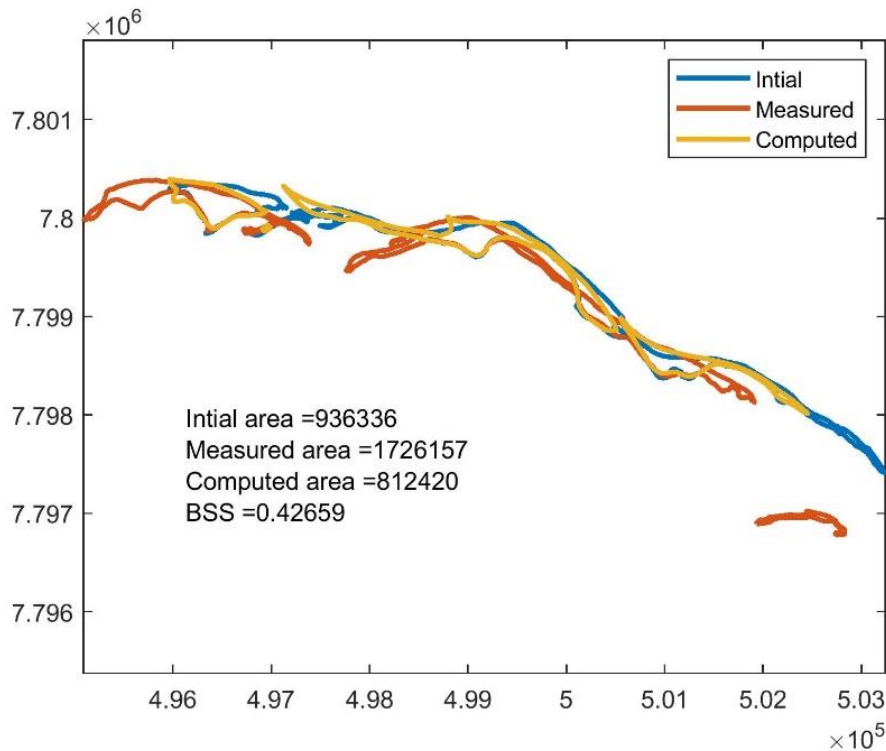
Figure 24 Stockton-Pole Islands, result no. 1, initial shoreline (blue) at 2000 , measured (red) and computed (yellow) at 2010.

As shown in Figure 24, the computed shorelines remained stable and reproduced neither the breaching in the middle nor the spit growing to the west. However, the BSS value is more than 0.4 but does not represent a proper matching between the computed and the measured shorelines.

4.5   Additional sensitivity tests

Additional sensitivity tests were performed for two reasons: first, in the previous simulations the actual dates of the initial and final shorelines were unknown exactly to which year in the 2000s and 2010s they belong, so it was assumed to start at 2000 and 2010. However, after extracting the shorelines at 2000 and 2010 using CoasSat, it was found that the assumption is not accurate. Instead, accurate dates will reduce the uncertainty of the results.

Second, a specific period from 2006 to 2009 was chosen because of (clearly) spits growing in such a short period; also the wave conditions (Figure 7), probably the highest within the

available data period, played an important role in the dynamic changes.
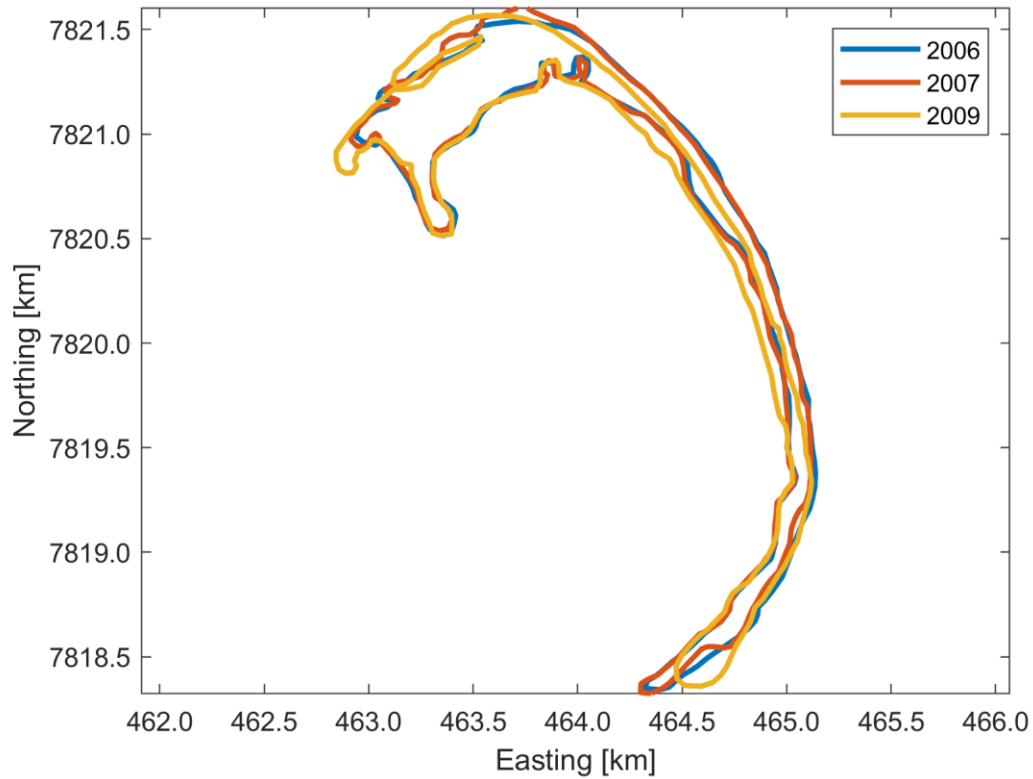
Figure 25 Cross Island shorelines: 2006 (blue), 2007 (red), and 2009 (yellow), the shorelines were extracted using CoastSat.

A reduced number of values were tried based on what showed better results in the previous simulations; the focus was to question the following points: the effect of reducing the surf width on the spit direction, how the two upwind correction approaches and the smooth factor affect the shape of the spit, and the best combination between the depth of closure, spit width, barrier height and alongshore formula parameter b. More than 500 simulations were performed with different combinations. In Table 4-5, a number of simulations inputs are presented, while few results were not presented because of having same results (e.g. using surf width equal to 50 or 100 m gives same results as 200 m) or failed to complete the simulation.

Table 4-5 Cross Island simulation trials using CoastSat shorelines

No.	b [10^6]	D_C	Two points	spit width	smooth Factor	surf width	OWscale	Barrier height	BSS	Total Area
3	0,1	5	2	250	0,05	200	0,0001	1	0,0576	742315
4	0,1	5	1	250	0,05	200	0,0001	1	0,0183	736313
5	0,1	5	2	250	0,05	200	0,0001	1,5	0,0576	742315
6	0,1	5	1	250	0,05	200	0,0001	1,5	0,0183	736313
7	0,1	5	2	250	0,05	200	0,0001	1	-0,2540	730655
8	0,1	5	1	250	0,05	500	0,0001	1	-0,2800	741344

9	0,1	5	2	250	0,05	500	0,0001	1,5	-0,2540	730655
10	0,1	5	1	250	0,05	500	0,0001	1,5	-0,2800	741344
19	0,1	5	2	250	0,1	200	0,0001	1	0,1019	743945
20	0,1	5	1	250	0,1	200	0,0001	1	0,0685	743490
21	0,1	5	2	250	0,1	200	0,0001	1,5	0,1019	743945
22	0,1	5	1	250	0,1	200	0,0001	1,5	0,0685	743490
23	0,1	5	2	250	0,1	500	0,0001	1	-0,4767	731296
24	0,1	5	1	250	0,1	500	0,0001	1	-0,3585	735772
25	0,1	5	2	250	0,1	500	0,0001	1,5	-0,4767	731296
26	0,1	5	1	250	0,1	500	0,0001	1,5	-0,3585	735772
32	0,1	5	2	300	0,05	200	0,0001	1	0,0558	741058
33	0,1	5	1	300	0,05	200	0,0001	1	0,0316	736403
34	0,1	5	2	300	0,05	200	0,0001	1,5	0,0558	741058
35	0,1	5	1	300	0,05	200	0,0001	1,5	0,0316	736403
36	0,1	5	2	300	0,05	200	0,0001	1	-0,2245	730657
37	0,1	5	1	300	0,05	500	0,0001	1	-0,2674	743764
38	0,1	5	2	300	0,05	500	0,0001	1,5	-0,2245	730657
39	0,1	5	1	300	0,05	500	0,0001	1,5	-0,2674	743764
48	0,1	5	2	300	0,1	200	0,0001	1	0,1176	743861
49	0,1	5	1	300	0,1	200	0,0001	1	0,0523	738020
50	0,1	5	2	300	0,1	200	0,0001	1,5	0,1176	743861
51	0,1	5	1	300	0,1	200	0,0001	1,5	0,0523	738020
52	0,1	5	2	300	0,1	500	0,0001	1	-0,4114	737251
53	0,1	5	1	300	0,1	500	0,0001	1	-0,2395	735220
54	0,1	5	2	300	0,1	500	0,0001	1,5	-0,4114	737251
55	0,1	5	1	300	0,1	500	0,0001	1,5	-0,2395	735220
64	0,1	10	2	250	0,05	200	0,0001	1	0,1330	745306
65	0,1	10	1	250	0,05	200	0,0001	1	0,1595	750839
66	0,1	10	2	250	0,05	200	0,0001	1,5	0,1330	745306
67	0,1	10	1	250	0,05	200	0,0001	1,5	0,1595	750839
68	0,1	10	2	250	0,05	200	0,0001	1	0,0031	740584
69	0,1	10	1	250	0,05	500	0,0001	1	-0,0545	741405
70	0,1	10	2	250	0,05	500	0,0001	1,5	0,0031	740584
71	0,1	10	1	250	0,05	500	0,0001	1,5	-0,0545	741405
80	0,1	10	2	250	0,1	200	0,0001	1	0,1547	749451
81	0,1	10	1	250	0,1	200	0,0001	1	0,1734	747519
82	0,1	10	2	250	0,1	200	0,0001	1,5	0,1547	749451
83	0,1	10	1	250	0,1	200	0,0001	1,5	0,1734	747519
84	0,1	10	2	250	0,1	500	0,0001	1	0,0412	744590
85	0,1	10	1	250	0,1	500	0,0001	1	-0,0172	744289
86	0,1	10	2	250	0,1	500	0,0001	1,5	0,0412	744590

87	0,1	10	1	250	0,1	500	0,0001	1,5	-0,0172	744289
96	0,1	10	2	300	0,05	200	0,0001	1	0,1464	745219
97	0,1	10	1	300	0,05	200	0,0001	1	0,1757	747839
100	0,1	10	2	300	0,05	200	0,0001	1	0,0303	740304
101	0,1	10	1	300	0,05	500	0,0001	1	-0,0378	741480
112	0,1	10	2	300	0,1	200	0,0001	1	0,1746	749296
113	0,1	10	1	300	0,1	200	0,0001	1	0,1925	747269
116	0,1	10	2	300	0,1	500	0,0001	1	0,0658	743401
117	0,1	10	1	300	0,1	500	0,0001	1	-0,0095	743241
128	0,1	15	2	250	0,05	200	0,0001	1	0,1355	747708
129	0,1	15	1	250	0,05	200	0,0001	1	0,1376	747727
132	0,1	15	2	250	0,05	200	0,0001	1	0,0573	744901
133	0,1	15	1	250	0,05	500	0,0001	1	0,0912	743268
144	0,1	15	2	250	0,1	200	0,0001	1	0,1619	749221
145	0,1	15	1	250	0,1	200	0,0001	1	0,1542	750351
148	0,1	15	2	250	0,1	500	0,0001	1	0,0832	743914
149	0,1	15	1	250	0,1	500	0,0001	1	0,107	742683
160	0,1	15	2	300	0,05	200	0,0001	1	0,158	747893
161	0,1	15	1	300	0,05	200	0,0001	1	0,1626	747547
164	0,1	15	2	300	0,05	200	0,0001	1	0,0756	744650
165	0,1	15	1	300	0,05	500	0,0001	1	0,1084	742884
176	0,1	15	2	300	0,1	200	0,0001	1	0,1846	749084
177	0,1	15	1	300	0,1	200	0,0001	1	0,1802	749843
180	0,1	15	2	300	0,1	500	0,0001	1	0,1043	743379
181	0,1	15	1	300	0,1	500	0,0001	1	0,1208	742395
187	0,1	5	2	250	0,05	200	0,0001	1	0,107	742683
188	0,1	5	2	250	0,05	200	0,0001	1	0,0832	743914
194	0,5	5	2	250	0,05	200	0,0001	1	-1,5781	594094
195	0,5	5	1	250	0,05	200	0,0001	1	-0,7027	606439
198	0,3	5	2	250	0,05	200	0,0001	1	-0,4478	732502
199	0,3	10	2	250	0,05	200	0,0001	1	-0,5114	732953
200	0,3	5	2	250	0,05	200	0,0001	1	-3,0584	397796
207	0,4	10	2	250	0,05	200	0,0001	1,5	-0,7721	712679
208	0,2	10	2	250	0,05	200	0,0001	1,5	-0,454	729614
210	0,2	10	1	250	0,05	200	0,0001	1,5	-0,8801	730739
211	0,2	10	2	300	0,05	200	0,0001	1	-0,2051	731055
212	0,2	10	1	300	0,05	200	0,0001	1	-0,2474	729998
213	0,2	10	2	300	0,05	200	0,0001	1,5	-0,2051	731055
214	0,3	10	2	250	0,05	150	0,0001	1,5	-0,3361	724483
215	0,3	10	1	250	0,05	150	0,0001	1	-0,0882	725974
216	0,3	10	2	250	0,05	150	0,0001	1	-0,2922	725941

217	0,3	10	1	250	0,05	150	0,0001	1	-0,317	722223
251	0,3	15	2	250	0,05	200	0,0001	1	0,06	737990
252	0,3	15	1	250	0,05	200	0,0001	1	0,0829	727360
255	0,3	15	2	250	0,05	200	0,00001	1	0,0232	739462
256	0,3	15	1	250	0,05	200	0,00001	1	9,79E-05	730575
259	0,3	15	2	250	0,05	500	0,0001	1	-0,6958	727785
270	0,3	15	1	250	0,05	500	0,0001	1	-0,3516	715060
271	0,1	10	1	250	0,05	200	0,00001	1	0,1124	737202
272	0,1	10	1	250	0,05	200	0,00001	1	-1,1836	744897
273	0,1	10	1	250	0,05	150	0,00001	1	-0,1087	739987
274	0,1	10	1	250	0,05	150	0,0001	1	-0,028	740637
279	0,3	10	1	250	0,05	200	0,00001	1	-0,2254	708711
280	0,3	10	1	250	0,05	200	0,0001	1	-0,8147	750228
281	0,3	10	1	250	0,05	150	0,00001	1	-0,2103	719638
285	0,4	10	1	250	0,1	150	0,00001	1	0,0216	718898
286	0,4	10	2	250	0,2	150	0,00001	1	-1,5293	703457
433	0,1	5	1	250	0,05	150	0,0001	1,5	-2,2294	727451
434	0,1	5	2	250	0,05	100	0,0001	1,5	-1,415	735587
435	0,1	5	1	250	0,05	100	0,0001	1,5	-2,2294	727451
436	0,1	10	2	250	0,05	150	0,0001	1,5	-0,5681	740623
437	0,1	10	1	250	0,05	150	0,0001	1,5	-0,5312	741215
438	0,1	10	2	250	0,05	100	0,0001	1,5	-0,5681	740623
439	0,1	10	1	250	0,05	100	0,0001	1,5	-0,5312	741215
440	0,3	5	2	250	0,05	150	0,0001	1,5	-3,0843	696093
441	0,3	5	1	250	0,05	150	0,0001	1,5	-1,4762	656699
442	0,3	5	2	250	0,05	100	0,0001	1,5	-3,0843	696093
443	0,3	5	1	250	0,05	100	0,0001	1,5	-1,4762	656699
444	0,3	10	2	250	0,05	150	0,0001	1,5	-0,3313	724483
445	0,3	10	1	250	0,05	150	0,0001	1,5	-0,0843	725974
446	0,3	10	2	250	0,05	100	0,0001	1,5	-0,3313	724483
447	0,3	10	1	250	0,05	150	0,0001	1,5	-0,0843	725974
449	0,3	15	2	250	0,05	250	0,0001	1,25	-0,0256	738826
450	0,3	15	1	250	0,05	250	0,0001	1,25	-0,1777	741921
451	0,3	15	2	250	0,01	250	0,0001	1,25	-0,2257	739762
452	0,3	15	1	250	0,01	250	0,0001	1,25	-0,1811	741728
453	0,3	10	2	250	0,05	250	0,0001	1,25	-0,1967	727676
454	0,3	10	1	250	0,05	250	0,0001	1,25	-0,2716	733338
455	0,3	10	2	250	0,01	250	0,0001	1,25	-0,7369	731760
456	0,3	10	1	250	0,01	250	0,0001	1,25	-0,3951	734504
457	0,5	15	2	250	0,05	250	0,0001	1,25	-0,4652	721705
458	0,5	15	1	250	0,05	250	0,0001	1,25	-0,3942	719893

459	0,5	15	2	250	0,01	250	0,0001	1,25	-0,4602	734050
460	0,5	15	1	250	0,01	250	0,0001	1,25	-0,3669	733156
461	0,5	10	2	250	0,05	250	0,0001	1,25	-1,2531	705023
462	0,5	10	1	250	0,05	250	0,0001	1,25	-1,2287	677760
463	0,5	10	2	250	0,01	250	0,0001	1,25	-2,6359	725931
464	0,5	10	1	250	0,01	250	0,0001	1,25	-1,8362	729624
465	0,3	15	2	250	0,05	200	0,0001	1,25	0,0576	742315
466	0,3	15	1	250	0,05	200	0,0001	1,25	0,0183	736313
467	0,3	15	2	250	0,01	200	0,0001	1,25	0,0271	741639
468	0,3	15	1	250	0,01	200	0,0001	1,25	0,0369	743896
469	0,3	10	2	250	0,05	200	0,0001	1,25	-0,0456	738264
470	0,3	10	1	250	0,05	200	0,0001	1,25	-0,3001	734595
471	0,3	10	2	250	0,01	200	0,0001	1,25	-0,1442	738534
472	0,3	10	1	250	0,01	200	0,0001	1,25	-0,2597	735430
473	0,5	15	2	250	0,05	200	0,0001	1,25	-0,1835	726991
474	0,5	15	1	250	0,05	200	0,0001	1,25	-0,3643	723025
475	0,5	15	2	250	0,01	200	0,0001	1,25	-0,6058	737787
476	0,5	15	1	250	0,01	200	0,0001	1,25	-0,5153	735202
477	0,5	10	2	250	0,05	200	0,0001	1,25	-1,259	705211
478	0,5	10	1	250	0,05	200	0,0001	1,25	-0,133	710218
479	0,5	10	2	250	0,01	200	0,0001	1,25	-1,9654	735552
480	0,5	10	1	250	0,01	200	0,0001	1,25	-0,6366	720240

The simulations showed that the surf width is affecting the spit direction, using smaller values (closer surf width) means more refracted waves, lower wave heights and wave directions oriented more toward the perpendicular direction on the shoreline. However, all values less than 200 m lead to the same result. Most probably because the 200 m is the grid size of the bathymetry used for the wavetable.

The highest BSS value is 0.19255 (Figure 26); however, other simulations receiving lower BSS show better matching between the shorelines, especially in the northern area.
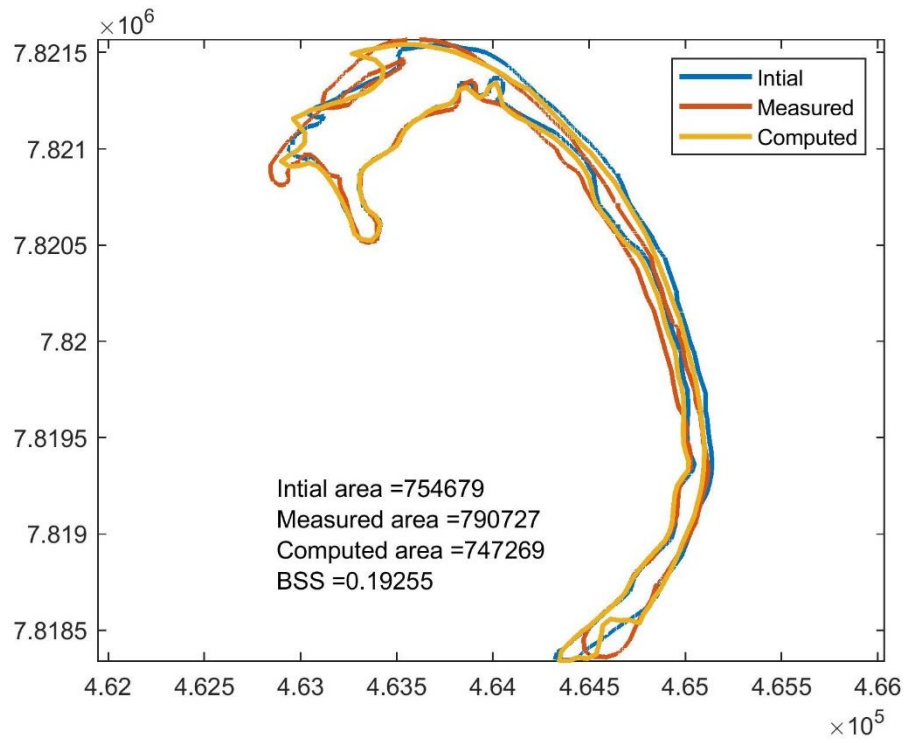
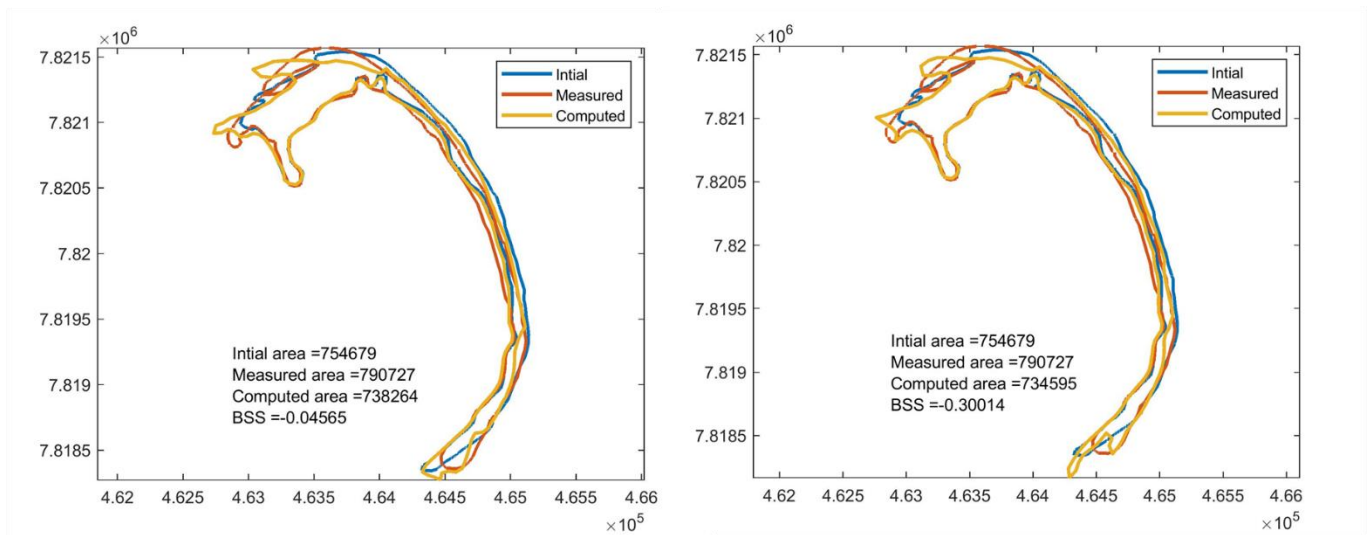Figure 26 Cross Island (2006-2009): results no. 113.

Figure 27 Cross Island (2006-2009): left panel result no. 469, right panel result no. 470.

5 Preliminary conclusions and Future study

5.1 Conclusions

Based on the results presented in this report, the following conclusions can be drawn:

- Alongshore transport, one of the main controlling processes, is controlled by two parameters the closure depth and the calibration factor b; both play an essential role; however, the process could be controlled with one of them.
- Using the 2D wave refraction solver and the bathymetry update routine developed within this project leads to more stable and realistic results.
- The barrier overwash routine has shown its capability to represent the barrier island rollover process, also to increase the surface area. However, the migration direction is not accurate.
- Both upwind correction methods produce slightly different spit shapes; the first method appears to give more stable and realistic shapes. However, further validation tests with longer simulation are necessary in order to draw a final conclusion.
- Although the model captures the spit growth and migration, the field observations show that the spit growth is built from smaller layers of small spits that grow over the time, which is not captured in the model.
- Regarding the spit growth direction, the decrease in surf width value leads to more refraction of the approaching waves leading to more correction of the spit orientation.
- Using wave time series leads to more realistic results than using schematized wave climates.
- The total computed area is always smaller compared to the field observations.
- The method of calculating BSS in this study does not represent the model performance correctly in some cases.

5.2 Recommendations

- The different alongshore transport formulas should be further tested and their effect on the spit orientation checked.
- The wave climate schematization should be re-assessed as the wave input by increasing the number of directional and wave height bins (intervals).
- Since the spit direction was affected by the surf width till the value (200 m) which is equal to the grid size of the bathymetry used in the wavetable, and the spits are not growing in the right direction, the use of finer grid size around the shoreline might improve the spit direction.

5.3 Future study

- Including the ice effect

Ice-push and ice override events transport and erode a significant amount of sediment on islands and coastal regions across the Beaufort Sea. Ice push occurs when ice blocks, forced onshore by strong winds or currents, push sediment into ridges farther inland (Craig et al., 1985). On the outer barrier islands such as Narwhal and Cross Islands, ice-push ridges up to 2.5 meters and 100 meters inshore from the beach have been identified (Hopkins & Hartz, 1978). Therefore, the impact of the ice should be included in the model, in order to be able to quantify the driving forces of coastal changes.

- Extract additional data from satellite images

As the shorelines extracted from the satellite images helped in the first phase, additional data could be extracted from the satellite images (e.g. beach slopes (Vos et al., 2020), bathymetry (Gebco, 2019)).

- Investigating how each process contributes to the shoreline changes

Since there are available shorelines every year, also the wave data, then the data could be analysed together to quantify how each process (or driving force) contributes to the shoreline changes. One approach could be: using the available wave conditions; the wave energy will be calculated, also the alongshore transport could be calculated using the model, then the effect of the wave on the rollover could be estimated.

- Apply data assimilation in ShorelineS

Data assimilation has been well established in coastal science (e.g. ocean and wave prediction) as a means to combine inaccurate models and data to calibrate model parameters automatically and to provide optimized forecasts including error estimates. Long and Plant (2012) introduced extended Kalman filtering to the domain of coastline evolution modelling, and Vitousek et al. (2017) applied it in an advanced coastline model for the state of California. Vitousek et al. (submitted) presented an ensemble Kalman filter shoreline model to predict the coastline evolution due to waves and sea-level. A recent modelling competition (Montaño et al., 2020) showed that using machine learning techniques to reproduce shoreline changes is better than normal models.
A data assimilation scheme should be developed allowing an automated process of the (large amount of) available data to auto-calibrate the model, and as a result, not only the result will improve but also the uncertainty will reduce.

6 References

Ashton, A. D., & Murray, A. B. (2006). High-angle wave instability and emergent shoreline shapes: 1. Modeling of sand waves, flying spits, and capes. *Journal of Geophysical Research: Earth Surface*, *111*(4), 1–19. https://doi.org/10.1029/2005JF000422

Ashton, A. D., Murray, A. B., & Arnoult, O. (2001). Formation of coastline features by large-scale instabilities induced by high-angle waves. *Nature*, *414*(6872), 296–300. https://doi.org/10.1038/415666a

Benedet, L., Dobrochinski, J. P. F., Walstra, D. J. R., Klein, A. H. F., & Ranasinghe, R. (2016). A morphological modeling study to compare different methods of wave climate schematization and evaluate strategies to reduce erosion losses from a beach nourishment project. *Coastal Engineering*, *112*, 69–86. https://doi.org/10.1016/j.coastaleng.2016.02.005

Birkemeier, W. A. (1985). Field data on seaward limit of profile change. *Journal of Waterway, Port, Coastal and Ocean Engineering*, *111*(3), 598–602. https://doi.org/10.1061/(ASCE)0733-950X(1985)111:3(598)

Brutsché, K. E., Rosati, J., & Pollock, C. E. (2014). Calculating depth of closure using WIS hindcast data. Vicksburg, Mississippi: U.S. Army Engineer Research and Development Center.

Craig, J. D., Sherwood, K. w., & Johnson, P. P. (1985). *Beaufort sea planning area; Alaska*.

Dean, R. G. (1991). Equilibrium beach profiles : characteristics and applications. *Journal of Coastal Research*, *7*(1), 53–84.

Gebco, I. (2019). The IHO-IOC GEBCO Cook Book. IHO Publication B-11.

Gibbs, A. E., & Richmond, B. M. (2015). *National Assessment of Shoreline Change — Historical Shoreline Change Along the North Coast of Alaska , U. S.-Canadian Border to Icy CapeCape: U.S. Geological Survey Open-File Report 2015–1048*. Virginia. https://doi.org/10.3133/ofr20151048.

Gibbs, A. E., Richmond, B. M., Erikson, L., & Jones, B. (2018). Arctic Alaska's barrier islands: Morphological types and historical change. *AGU Fall Meeting Abstracts*, *December*. Retrieved from https://ui.adsabs.harvard.edu/abs/2018AGUFMEP23D2353G

Hallermeier, R. J. (1981). A profile zonation for seasonal sand beaches from wave climate. *Coastal Engineering*, *4*, 253–277.

Hopkins, D. M., & Hartz, R. W. (1978). *Coastal Morphology, Coastal Erosion, and Barrier Islands of the Beaufort Sea, Alaska*.

Kaergaard, K., & Fredsoe, J. (2013). A numerical shoreline model for shorelines with large curvature. *Coastal Engineering*, *74*, 19–32. https://doi.org/10.1016/j.coastaleng.2012.11.011

Kamphuis, J. w. (1992). Computation of coastal morphology. *Icce*, 211–257.

Long, J. W., & Plant, N. G. (2012). Extended Kalman Filter framework for forecasting shoreline evolution. *Geophysical Research Letters*, *39*(13), 1–6. https://doi.org/10.1029/2012GL052180

Montaño, J., Coco, G., Antolínez, J. A. A., Beuzen, T., Bryan, K. R., Cagigal, L., … Vos, K. (2020). Blind testing of shoreline evolution models. *Scientific Reports*, *10*(1), 1–10.

https://doi.org/10.1038/s41598-020-59018-y

Robinet, A., Idier, D., Castelle, B., & Marieu, V. (2018). A reduced-complexity shoreline change model combining longshore and cross-shore processes: The LX-Shore model. *Environmental Modelling and Software*, *109*(August), 1–16. https://doi.org/10.1016/j.envsoft.2018.08.010

Roelvink, D., Huisman, B., Elghandour, A., Ghonim, M., & Reyns, J. (2020). Efficient modeling of complex sandy coastal evolution at monthly to century time scales. *Frontiers in Marine Science*, *7*, 535. https://doi.org/10.3389/fmars.2020.00535

Sutherland, J., Peet, A. H., & Soulsby, R. L. (2004). Evaluating the performance of morphological models. *Coastal Engineering*, *51*(8–9), 917–939. https://doi.org/10.1016/j.coastaleng.2004.07.015

USACE. (1984). *Shore Protection Manual*. *Coastal Engineering Research Center* (Vol. 1). US Army Corps of Engineers, Waterways Experiment Station; Coastal Engineering Research Center; Vicksburg; Miss. https://doi.org/10.5962/bhl.title.47830

van Rijn, L. C., Wasltra, D. J. R., Grasmeijer, B., Sutherland, J., Pan, S., & Sierra, J. P. (2003). The predictability of cross-shore bed evolution of sandy beaches at the time scale of storms and seasons using process-based profile models. *Coastal Engineering*, *47*(3), 295–327. https://doi.org/10.1016/S0378-3839(02)00120-5

Vitousek, S., Barnard, P. L., Limber, P., Erikson, L., & Cole, B. (2017). A model integrating longshore and cross-shore processes for predicting long-term shoreline response to climate change. *Journal of Geophysical Research: Earth Surface*, *122*(4), 782–806. https://doi.org/10.1002/2016JF004065

Vitousek, S., Cagigal, L., Montaño, J., Rueda, A., Mendez, F., & Barnard, P. L. (2020). The application of ensemble wave forcing to quantify uncertainty of shoreline change models. *Journal of Geophysical Research: Earth Surface*, ((().

Vos, K., Harley, M. D., Splinter, K. D., Walker, A., & Turner, I. L. (2020). Beach slopes from satellite-derived shorelines. *Geophysical Research Letters*.

Vos, K., Splinter, K. D., Harley, M. D., Simmons, J. A., & Turner, I. L. (2019). CoastSat : A Google Earth Engine-enabled Python toolkit to extract shorelines from publicly available satellite imagery. *Environmental Modelling and Software*, *122*, 104528. https://doi.org/10.1016/j.envsoft.2019.104528